ON FABRICATION AND CORROSION RESISTANCE OF SUPER-HYDROPHOBIC 17-4 PH STAINLESS STEEL SURFACES

by

© Mona Amiriafshar

A Thesis submitted to the
School of Graduate Studies
in partial fulfillment of the requirements for the degree of

Master of Engineering

Faculty of Engineering and Applied Science

Memorial University of Newfoundland

Nov. 2019

St. John’s Newfoundland

*"Dedicated to my best friend, **Mehran**, and my parents"*

Abstract

Fabrication of surfaces with hydrophobic and super-hydrophobic property has drawn extensive interests as a solution to protect metal surfaces from corrosion attacks, with potential applications in cooling devices for electronics, microfluidic systems for controlled drug delivery, as well as anti-icing, and self-cleaning techniques. This study addresses the impact of surface wettability, *i.e.*, hydrophobicity and super-hydrophobicity, on corrosion resistance improvement of metallic materials. Hydrophobic and super-hydrophobic metal surfaces are desirable to minimize the adhesion between water droplets and the surface. This thesis aims to fabricate and investigate 17-4 PH stainless steel surfaces with lowered surface energies and modified wetting properties. Various micro- and sub-micro scale finished surfaces with different surface roughness, namely as-received, sandblasted, ground, and polished, were employed, followed by applying a low energy super-hydrophobic and Zn electrodeposition coatings on 17-4 PH stainless steel base material to fabricate hydrophobic and super-hydrophobic surfaces, respectively. The specific impacts of the surface roughness on wettability, corrosion resistivity, and coating adhesion of the manufactured surfaces were examined. The coated 17-4 PH stainless steel surfaces were found effective in preventing the aggressive chloride ions from approaching the substrate, leading to the improved corrosion performance of the material. Moreover, the initial surface roughness of the material was found to be a dominating factor in controlling the uniformity and adhesion durability of the coated substrates.

Keywords: (Super)hydrophobic surface, Stainless steel, Surface roughness, Wettability, Zinc electrodeposition, Coating Adhesion

Acknowledgements

I would like to thank my supervisors Drs. Ali Nasiri and Xili Duan for their expert advice, constant encourage, and unlimited support during the process of my thesis work.

I would like to thank my colleagues and friends for their wonderful collaboration and brilliant ideas. Without your support, I could not make such impressive achievement in my research work.

This project would have been impossible without the financial support from Petroleum Research Newfoundland & Labrador (PRNL) and Memorial University of Newfoundland (MUN). Moreover, I especially want to thank Department of Mechanical Engineering at MUN for providing excellent resources to support my research.

Table of contents

List of Figures

List of Tables

List of Abbreviations and Symbols

γ_{la}	Interfacial Energy Between Liquid and Air
γ_{ls}	Interfacial Energy Between Solid and Liquid
γ_{sa}	Interfacial Energy Between Air and Solid
CBM	Coated Base Metal
CE	Counter Electrode
CG	Coated Ground
CP	Coated Polished
CPE	Constant Phase Element
CPE_c	Coating Constant Phase Element
CPE_p	Constant Phase Element of The Passive Layer
CPP	Cyclic Potentiodynamic Polarization
CSB	Coated Sandblasted
EDX	Energy Dispersive X-ray
EEC	Equivalent Electrical Circuit
EIS	Electrochemical Impedance Spectroscopy
E_{pit}	Pitting Potential
$E_{rep.}$	Re-Passivation Potential
f	Liquid Contact Area Fraction
I_{corr}	Corrosion Current Density
OCP	Open Circuit Potential
PH	Precipitation-Hardening
R_a	Average Surface Roughness

R_c	Coating Resistance
R_{ct}	Charge Transfer Resistance
RE	Reference Electrode
R_f	Passive Layer Resistance
R_p	Polarization Resistance
R_s	Describes The Solution Resistance
SE	Secondary Electrons
SEI	Secondary Electron Imaging
SS	Stainless Steel
WE	Working Electrode
XRD	X-ray Diffraction
Z	Impedance
θ	Contact Angle
θ_e	Intrinsic Contact Angle
θ_r^c	Apparent Contact Angle

CHAPTER 1

1. Introduction

1.1. Background

Hydrophobic and super-hydrophobic surfaces on metal substrates are widely used for many industrial applications due to their low-cost, simplicity in preparation, and good performance. Different fabrication techniques have been developed in preparing hydrophobic surfaces on metals, such as applying low surface energy coatings and/or developing micron/sub-micron scale textures on the surface. Different types of coating materials have been developed for producing hydrophobic and super-hydrophobic surfaces, which can be categorized into organic coatings and inorganic coatings [1]. However, the main limitations of the (super)hydrophobic coatings are their low durability and high production costs [2]. The other utilized method to develop a hydrophobic surface is based on fabrication of optimum sized micron/sub-micron superficial roughness capable of maintaining air pockets, leading to a decreased contact area between the solid and liquid surfaces [3]. The resultant hydrophobic property was ascribed to the effects of the laser-induced roughness and low surface energy resulting from the coating [4]. This created air pockets between water droplets and the surface, as a result of surface treatment leading to super-hydrophobicity with a very high apparent static contact angle. It has been reported that laser textured surface of 17-4 PH stainless steel with 50-100 μm channels size followed by the hydrophobic coating resulted in contact angles of 145°, while the non-textured coated base metal displayed the contact angle of 121° [4]. Another study on the same material showed that the measured static contact angles of the pillar and channeled surfaces with the size in order of 50 μm are over 130° without any coating, compared with 70° on the original 17-4 PH stainless steel surface before laser machining [3].

However, the prolonged processing time and the high fabrication cost of all these surface treatment processes would restrict their potential application for large-scale engineering components. Therefore, in this study, to fabricate the required surface features to induce hydrophobic and super-hydrophobic properties on the surface, the fast and cost-effective conventional surface treatment procedures, including sandblasting, grinding, and polishing, were adopted. This thesis is aimed to fabricate super-hydrophobic 17-4 PH stainless steel surfaces through different surface treatment methods coupled with applying a super-hydrophobic coating and Zinc electrodeposition. The effectiveness of the fabricated surfaces in protection against corrosion and the electrochemical stability of the substrate will also be investigated [5].

1.2. Research objective

Fabrication of surfaces with hydrophobic and super-hydrophobic property has attracted extensive attention as a solution to preserve metal surfaces in corrosive attacks, with potential in a broad range of applications. This thesis addresses the impact of hydrophobicity and super-hydrophobicity on corrosion resistance improvement and coating durability of 17-4 PH stainless steel, through the fabrication of lowered surface energies and modified wetting properties. Various micro- and sub-micro scale surface roughness, followed by applying low energy super-hydrophobic and Zinc electrodeposition coating, were employed to fabricate hydrophobic and super-hydrophobic surfaces on 17-4 PH stainless steel base material. The particular impacts of the initial surface roughness on the wetting behavior, coating adhesion, and corrosion performance of the manufactured surfaces were examined.

1.3. Organization of the thesis

In Chapter 2, some related research in the fabrication of the super-hydrophobic stainless steel surfaces through different surface treatment methods was reviewed, such as polishing, grinding, and sandblasting coupled with Zn electrodeposition coating as super-hydrophobic coatings. Moreover, an overview of basic knowledge on hydrophobic surfaces, wetting characteristics, and corrosion behavior is presented.

In Chapter 3, some experimental procedures and characterization methods are introduced. The general procedures for creating different surface roughness and electrodeposition are described with details. Some characterization methods, such as contact angle measurement, X-ray diffraction, scanning electron microscopy, and corrosion measurement tests, are introduced in terms of background knowledge and their basic applications.

In Chapter 4, the fabrication of super-hydrophobic 17-4 PH stainless steel surfaces through different surface treatment methods coupled with applying a super-hydrophobic coating was explained. The effectiveness of the fabricated surfaces in protection against corrosion and the electrochemical stability of the substrate was also investigated.

In Chapter 5, the impact of the substrate's surface roughness on coating adhesion was discussed, and its durability is substantial, particularly in the harsh marine environments was examined. Therefore, the impacts of initial surface roughness on the contact angle and adhesion of the Zn coating are investigated.

In Chapter 6, an overall conclusion of my whole research effort is provided, and some future work based on my current results was suggested.

CHAPTER 2

2. Literature Review

2.1. Materials for hydrophobic applications

Nowadays, a wide variety of materials have been employed to produce hydrophobic and super-hydrophobic characteristics on their surfaces, such as organic materials, which are generally hydrophobic by nature, and inorganic materials, such as metallic substrates with hydrophilic nature [1]. Also, various methods and procedures have been employed to produce hydrophobic and super-hydrophobic surfaces, including photolithography [6], electrodeposition [7], laser or Plasma processing [8], chemical etching [9], and additively deposition [10]. In general, metallic components, thanks to their outstanding mechanical, corrosion, and thermal properties have attracted more attention for the fabrication of hydrophobic and super-hydrophobic surfaces [11], [12].

Stainless steels are considered the most commonly used corrosion resistant materials with great mechanical and thermal properties are employed in countless applications as engineering components for various industrial sectors and environments. Precipitation-hardening (PH) stainless steels have been developed to provide high strength and toughness while maintaining a good corrosion resistance [13]. As compared to the other members of stainless steels families, they have higher strength than austenitic or ferritic stainless steels, while possessing a higher toughness and ductility than martensitic stainless steels [14]. 17-4 PH martensitic stainless steel has been called the “workhorse” of the PH stainless steels family by providing an outstanding combination of high strength, excellent corrosion resistance, and relatively simple heat treatment cycles [15]. The dominant microstructure of the 17-4 PH stainless steel is martensitic in solution annealed

condition, and typically undergoes precipitation hardening steps after any forming operation. The microstructure of the base material employed in this study has been shown to be composed of parallel lath of martensite and δ-ferrite [4].

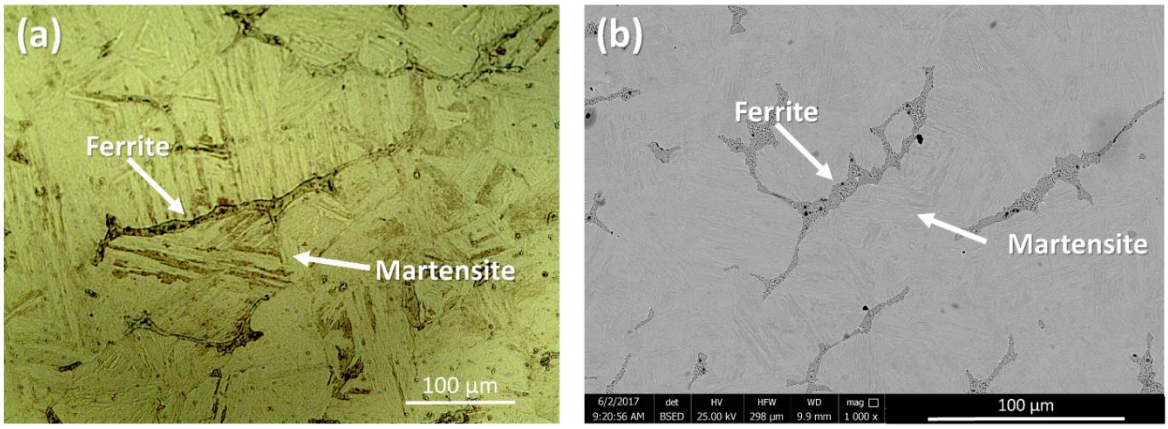

Figure 1. (a) the optical micrograph image and (b) the scanning electron microscope micrograph of as-received 17-4 PH stainless steel [4].

2.2. Corrosion

The term “Corrosion” that refers to the destructive electrochemical attack of a material [16], is a major challenge associated with harsh and aggressive environments, threatening and deteriorating the integrity and lifetime of the materials and structures [1]. There are various types of corrosion, each of which can be categorized by the purpose of the metal's chemical deterioration. General corrosion, localized corrosion, galvanic corrosion, environmental cracking, intergranular corrosion, and de-alloying are among the most important ones [17].

There are different standardized tests in corrosion resistance characterization, such as polarization methods such as potentiodynamic polarization and cyclic potential polarization, electrochemical impedance spectroscopy, as well as salt spray, providing knowledge regarding the

mechanisms of the corrosion, corrosion rate, and susceptibility of materials to the corrosion in different environments[16], [17].

In the Polarization techniques, the potential of the working electrode is changed, and the resultant current, which is produced as a function of time or potential, is monitored [18].

In the anodic polarization methods, the potential is turned in a more positive direction (anodic region), resulting in the electrons to be removed from the "anodic working electrode." On the other hand, in the cathodic polarization, the working electrode becomes more negative, and electrons are attached to its surface, causing electrodeposition. Cyclic polarization is performing the anodic and cathodic polarization in a cyclic manner[16], [17]. Therefore, this involves sweeping the potential in a positive direction until a predetermined rate of current or potential is achieved, then the scan is reversed toward more negative values until the initial value of potential is attained [17].

Electrochemical Impedance Spectroscopy (EIS) is a common quantitative technique for the accelerated evaluation of the anti-corrosion performance of protective coatings by determining the impedance of the electrochemical system as a function of frequency. EIS measurements also provide reliable data within short testing periods, providing the prediction of the long-term performance of the coatings [19].

The salt spray (or salt fog) corrosion test is a well-established test method applied to check corrosion resistance of materials (usually metallic, although stone, ceramics, and polymers may also be tested) and surface coatings. Salt spray experiment is an accelerated corrosion characterization test that produces a destructive attack to the coating of the samples in order to comparatively evaluate the appropriateness of the coating for application as a protective layer [20].

The protection against corrosion has been always one of the first priorities that should be considered from the design step, to the fabrication, operation, and maintenance of engineering components. One effective method for corrosion protection that has gained significant attention both from academia and industry in recent years is to create hydrophobic or super-hydrophobic properties on the surface of materials [4], [21], [22].

2.3. Wettability

Hydrophobic surfaces have a wetting contact angle higher than 90° degrees, while super-hydrophobic surfaces have noticeably higher water repellency with a wet contact angle of larger than 150° [23][21]. The contact angle can quantitively explain the wetting property of the solid surface. On an ideal smooth solid surface, Young's equation [24]:

$$\gamma_{sa} = \gamma_{ls} + \gamma_{la} \cos\theta$$

are applied to describe the relationship between the contact angle (θ) and three specific interfacial energies. As shown in Figure 2, the three interfacial energies, γ_{sa} (interfacial energy between air and solid), γ_{ls} (interfacial energy between solid and liquid), and γ_{la} (interfacial energy between liquid and air), should be balanced in the horizontal direction.

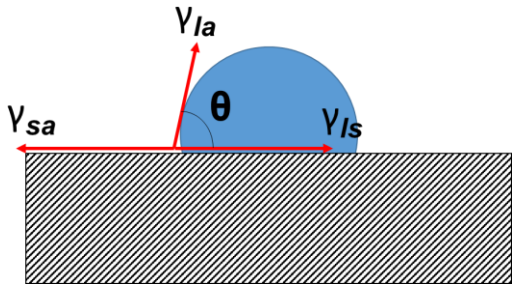

Figure 2. A schematic diagram of a droplet on a surface.

It has been reported that dominating factors in hydrophobicity are the surface roughness and surface energy [23], [25]. It is worth mentioning that surface energy, which principally is controlled by the surface's chemical composition, has more contribution to the hydrophobicity of the surface. However, the higher water repellency cannot be obtained without both minimizing the surface energy and tailoring the surface roughness [21]. Surface energy is also known as interfacial free energy, can be defined as the energy difference at the surface of the substrate compared to its bulk [26].

In recent years, controlling the water repellency of metal surfaces becomes a trendy research topic, as it could provide a solution to protect metal surfaces from corrosion attacks [27], [28]. Hydrophobic and super-hydrophobic surfaces on metal substrates are widely used for many industrial applications due to their low cost, simplicity in preparation, and good performance. Other benefits of hydrophobic surface in potential applications such as ice-covering proof [28], control of bio-fouling [1], self-cleaning [29], and drag reduction in fluid [30], makes it extremely useful for applying in corrosive environments, such as pipelines and marine industry.

Hydrophobic surfaces on metal substrates are widely used in industries and daily life because they have some unique properties. Currently, hydrophobic surfaces have already been applied in ice-covering-proof, self-cleaning, drag reduction in fluid flow, and so on.

Icing occurs at low temperatures, which can result in ice adhering to surfaces. Some outdoor setups have the requirement of ice-covering-proof, e.g., outdoor aerials at house roofs, solar panels, and power lines. Hydrophobic surfaces can efficiently reduce snow accumulation on the surface of outdoor setup and therefore relieve interference from the snow. Power lines can be sheared off due to ice and snow accumulation. When an airplane flies through a low-temperature zone, the accumulated ice on its surface is also a security threat [31]. Ice and snow accumulation

can also decrease the efficiency of wind turbines operating in a harsh environment like the polar regions [32].

Self-cleaning property is common in nature as well. For example, lotus leaf surfaces with a hierarchical structure and hydrophobic surface chemistry can provide high contact angles (>150°) and low hysteresis. The hierarchical surface features are important elements to obtain super-hydrophobicity [21]. These hierarchical surfaces are comprised of micro hills and valleys similar to the surface of a lotus leaf, or insect bodies [21], [33]. This property can make water droplets easily roll-off, pick up contaminants, and clean the path along [34]. This ability is called self-cleaning, also known as the lotus effect [2].

Drag reduction can be achieved by using micro-surface features and coating. This property has a broad range of applications, such as oil transportation and marine application [35]. Surface roughness can trap air and reduce the contact area between fluid and metal surfaces. The air layer is a kind of lubricating part that can lead to water slip, which is related to drag reduction. The role of coating on the surface is to reduce surface energy, which can help to achieve a higher contact angle [36]. Nowadays, many coating methods have been combined with micro- or nano-surface features on metal surfaces. Hydrophobic surfaces applied to microfluidic device or pipelines can reduce the pressure loss effectively. Tian *et al.* [37] found that the super-hydrophobic surface can reach a drag reduction benefit of up to 10 %. By comparing with the hydrophilic plate in the water channel, the suppression of coherent structure burst on the super-hydrophobic plate was found to achieve drag reduction. Besides the suppression of coherent structure burst, effective slip lengths were a critical factor that can help to achieve drag reduction. Truesdell *et al.* [38] found that coating and longitudinal grooves could be beneficial to increase slip lengths.

Hydrophobic and super-hydrophobic surfaces have also been found as a corrosion resistance enhancement solution on a wide variety of metallic substrates such as Al and Cu, and stainless steels. It has been reported by Boinovich *et al.* [39] that surface features created by nanosecond laser result in hydrophobic property of Al substrate. This consequently improves the pitting corrosion resistivity of Al in NaCl solution. Moreover, it was reported that applying fluoropolymer coatings on Cu surface resulting in the improving the corrosion performance of Cu, as evidenced by a significant reduction in corrosion current density as compared with the non-coated Cu surface, contributed to the formation of the insoluble diffusion barriers which could protect the substrate from the corrosive environment [11], [12]. Moreover, in the other study, the improvement in the corrosion performance of the 430 stainless steel was ascribed to the super-hydrophobicity of the surface, which has been resulted from the chemically etching surface. Moreover, Ng *et al.* [40] reported the improvement of the corrosion performance of the magnesium by applying the steric acid due to the barrier impact produced by the organic coating. The super-hydrophobic surface acts as a physical barrier between the metal substrate and the corrosive environment [41]. In a similar study also noted that more corrosion performance improvement could be obtained from super-hydrophobicity than that of hydrophobic surfaces [42]. Trdan *et al.* [43] also showed a direct correlation between the hydrophobicity and corrosion behavior by comparing the super hydrophilic and super-hydrophobic of the AISI316 L stainless steel surface.

The mechanism behind the improvement of the corrosion performance as a result of super-hydrophobicity was explained to be the retention of the air pocket layer on the metal surface, serving as a barrier and inhibiting the corrosion process from taking place [1]. Air pockets on the surface can improve the hydrophobicity since air is an extremely hydrophobic element with a contact angle of 180° [44].

Therefore, to improve the water repellency of the metallic surfaces, the commonly used fabrication techniques include either by the fabrication of micro or nano-scale surface features (so-called a tailored superficial roughness) [4], [5] or by reducing the surface energy through applying a low surface energy coating, or a combination of these two techniques [3], [4]. The surface roughness can create surface air packets between the water droplets and the surface, resulting in (super)hydrophobic behavior of the surface [4]. The surface roughness can be produced by removal techniques, such as chemical etching, laser texturing, and mechanical grinding [4], [5] [45]–[47], or additive methods, such as thermal evaporation and electrodeposition of a coating material [7], [48], [49].

2.4. Fabrication of hydrophobic and super-hydrophobic surfaces

A variety of surface treatments and materials removal strategies utilizing micro-electrical discharge machining (micro-EDM) [3] and laser surface treatments [4] have been used to fabricate micro/submicron-scale features on the metals surfaces to achieve low wettability. Different designs and features with various complexities, such as microscale channels, pillars [50], and sinusoidal patterns [51], all with excellent hydrophobic properties, were fabricated and studied so far. However, the prolonged processing time and the high fabrication cost of all these surface treatment methods would restrict their potential application for large-scale engineering components. Therefore, in order to fabricate the required surface features to induce hydrophobic and super-hydrophobic properties on the surface, fast and cost-effective surface treatment procedures, including sandblasting, grinding, and polishing, are highly favorable [5].

2.4.1. Sandblasting

In the sandblasting method, the abrasive particles impact on the sample's surface using high pressure compressed air. The response of the used abrasive particle size, the kinetic energy of the abrasive particles, and the standoff distance on the resultant roughness on various metallic surfaces have been examined by many researchers [52], [53]. Slatineanu *et al.* [53] demonstrated that the surface roughness criterions increase with the increase of the abrasive magnitudes and the kinetic energy of the abrasive particles.

2.4.2. Grinding and polishing

The grinding and polishing surface treatments also create various levels of surface roughness depends on the grit of the used abrasive sandpaper or the type of polishing pads and suspension, respectively. Consequently, sandblasting, grinding, and polishing methods can create different superficial roughness, which directly affects the surface wettability. Therefore, in this study, the impact of surface roughness on both wettability and corrosion performance of the 17-4 PH martensitic stainless steel will be addressed.

2.4.3. Electrodeposition

Moreover, among all additive-based strategies, electrodeposition is the most commonly used technique to fabricate a desired surface roughness [7], [54]. By adjusting the surface topography through creating a uniform micron- or nanoscale structure roughness on the surface, this method is capable of modifying the water repellent property of the surface [7]. Zinc has been generally used as a corrosion barrier coating to preserve a steel substrate surface from corrosive species [55], [56]. Steels are mainly composed of iron with a more positive standard reduction potential than Zinc, resulting in the sacrificial oxidization of zinc to protect the iron surface in an

ambient environment [57]. The electrodeposition of a Zinc layer on the surface has been also used as a viable method to fabricate super-hydrophobic surfaces in recent years [7], [22], [58]. For example, Zhang *et al.* [59] reported that the combination of zinc electrodeposition and an organic coating can induce super-hydrophobic properties on the surface.

2.5. Summary

This thesis aims to fabricate 17-4 PH stainless steel surfaces first through different surface treatment methods coupled with applying a super-hydrophobic coating and with lowered surface energies and modified wetting properties using a combination of Zinc electrodeposition and an organic coating and to further investigate the developed coating's electrochemical stability in a simulated marine environment. In the first project to fabricate the required surface features to induce hydrophobic and super-hydrophobic properties on the surface, the fast and cost-effective conventional surface treatment procedures, including sandblasting, grinding, and polishing, were adopted.

In the second project various micro- and sub-micron scale finished surfaces with different surface roughness, namely as-received, sandblasted, and ground, were employed, followed by zinc electrodeposition and applying the low energy super-hydrophobic coating (stearic acid) to fabricate hydrophobic and super-hydrophobic surfaces on 17-4 PH stainless steel base material. The impact of the substrate's surface roughness on coating adhesion and its durability is substantial, particularly in harsh marine environment. Therefore, despite a few existing studies on the fabrication of super-hydrophobic coating using Zn electrodeposition [7], [60], the impacts of initial surface roughness on the contact angle and adhesion of the Zn coating are still unknown and need to be investigated.

CHAPTER 3

3. Experimental Procedure

3.1. Material

Plates of martensitic type 17-4 PH stainless steel (SS) with nominal chemical composition of 16.70±0.05 wt.% Cr, 3.70±0.06 wt.% Ni, 2.91±0.07 wt.% Cu, Si and Mn ≤ 0.80 wt.%, and balance Fe were used in this study. The samples with the size of 6 mm thick × 8 mm wide × 50 mm long were prepared from the as-received material and used as the substrate material.

3.2. Surface Roughness

Several surface finishing procedures were applied on the as-received 17-4 PH stainless steel plate to produce samples with different superficial roughness. These include mechanical grinding using 500 grit SiC abrasive paper (provided the ground surface finish) and sandblasting utilizing aluminum oxide abrasive particle as the blasting media with the particle size of 70-80 mesh size (provided sandblasted surfaces). To remove any contaminants from the samples' surfaces prior to and after any surface treatment, the samples were cleaned ultrasonically in acetone and dried in air. The surface roughness of the fabricated samples was evaluated using a surface profilometer (Alpha-Step D-120 Stylus Profiler), shown in Figure 3.

A profilometer as a roughness measuring apparatus employed to quantify a surface's profile and its roughness. The critical component of the profilometer use in this study is a stylus with a 2-micron tip radius. Each surface was scanned employing the fine stylus at the scanning speed of 0.01 mm/s and the scanning step size of 0.04 μm. Moreover, the scan speed was set at 0.01 mm/s.

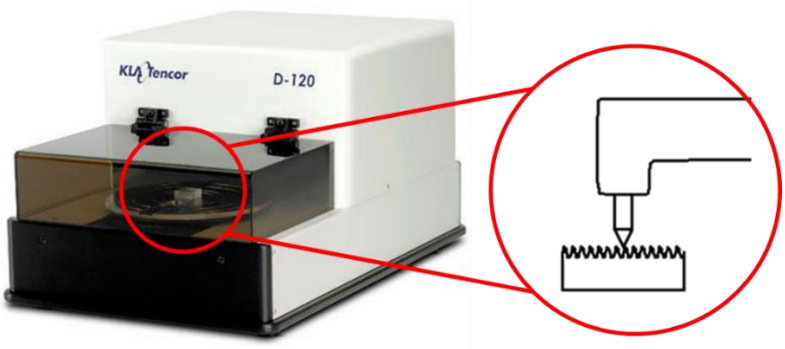

Figure 3. The Alpha-Step D-120 Stylus Profiler instrument

3.3. Coating methods

To prepare the hydrophobic and super-hydrophobic surfaces at different levels of surface roughness, the surface of the base metal was subjected to various surface finishing procedures, including mechanical grinding using 500 grit SiC abrasive paper (provided the ground surface finish), final polishing using a 0.02 µm alumina suspension (provided the polished surfaces) utilizing a Struers Tegramin-30 auto-grinder/polisher (Shown in Figure 4a), and sandblasting utilizing aluminum oxide abrasive particle as the blasting media with the particle sizes of 45-140 mesh, employing the SandStorm Edge–80410 micro-abrasive sandblaster shown in Figure 4b (provided sandblasted surfaces).

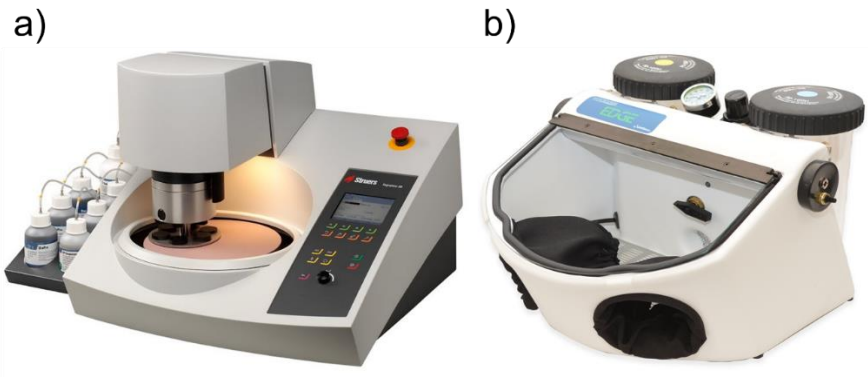

Figure 4. a) The Struers Tegramin-30 auto-grinder/polisher machine, b) the SandStorm Edge – 80410 micro-abrasive sandblaster [61], [62].

To remove any contaminants from the samples' surfaces prior to and after any surface treatment, the samples were cleaned ultrasonically in acetone and dried in air. Following this step and after fabrication of the ground, polished, and sandblasted surfaces, all samples, including the cleaned base metal with no pre-treatment (provided the base metal sample), were coated by applying 30-50 µm thick commercially available low-energy super-hydrophobic dip coating (FluoroThane WT) [63]. The cleaned samples' surfaces were immersed in the super-hydrophobic coating solution for 60 s, followed by removing the samples from the solution at a steady rate to ensure uniform coverage of the surface, and then dried in air.

3.4. Zinc electrodeposition

Zinc electrodeposition is the primary step in this study to fabricate the low water adhesion super-hydrophobic surfaces. The composition of the used electrolyte was 0.2 M $ZnCl_2$ and 3.5 M NH_4Cl in ultrapure water. According to the literature [7], [64], the Zn-NH_4Cl-NH_3-H_2O solution was selected as our electrolyte system for zinc electrodeposition. As shown in Figure 5, Zn electrodeposition process was conducted using a potentiostat unit, with the 17-4 PH stainless steel substrates as the working electrode (WE), a carbon rod as the counter electrode (CE), and a saturated silver/silver chloride (Ag/AgCl) as a reference electrode (RE). The deposition continued for 15 min at room temperature, while stirring the solution at 200 rpm. After the electrodeposition, the samples were immersed in a 0.05 M stearic acid organic coating solution ($C_{17}H_{35}COOH$) for 20 min. Then, the samples were taken out from the organic coating solution and dried in the air.

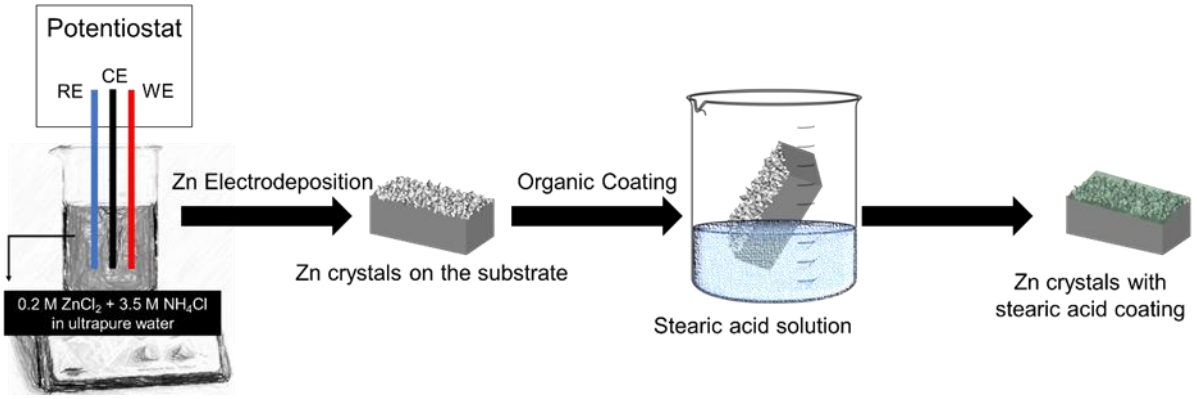

Figure 5. Schematic diagram of zinc electrodeposition process followed by applying the organic coating.

3.5. Wettability Measurements

The static contact angle measurement is the most straightforward and common technique to quantify the hydrophobicity or super-hydrophobicity of the fabricated surfaces. The wettability of the fabricated surfaces was characterized by measuring the distilled water droplets' contact angles on the surfaces, using an optical-based contact angle measuring system (Dataphysics OCA 15EC) shown at Figure 6 at room temperature to suppress the contamination of the surfaces. The Contact angle instrument has three essential elements, which are a sample stage, camera, and dosing system. To measure the static contact angle, a sample should be placed perfectly horizontally on the sample stage, and the camera should also be parallel to the sample surface. In order to make the droplet reach the sample surface, the needle was moved downward, without touching the needle tip to the surface, until the drop settles down to the sample's surface. Then the needle was raised while the droplet stays pinned on the surface. The analysis of the static contact angle follows three steps: Finding the baseline between the water droplet and the surface, detecting the drop contour, and calculating the contact angle by averaging the left contact angle and the right contact angle of each droplet, which are auto made by the software.

For accurate measurement of the static contact angles, the samples were laid flat on the sample holder with proper alignment with the equipment's digital camera. Using a micro-syringe, a 10 µl water droplet was dispensed on each surface and analyzed using the system's software. The water droplet's shape and its static contact angles were measured, employing the camera and the software's auto-calculation features. The water dispense rate was 2 µl/s, and the sessile drop diameter was about 1.4 mm. The contact angle measurement values were averaged over at least five different randomly selected points on each sample to account for any topography and chemical inhomogeneity on the surface.

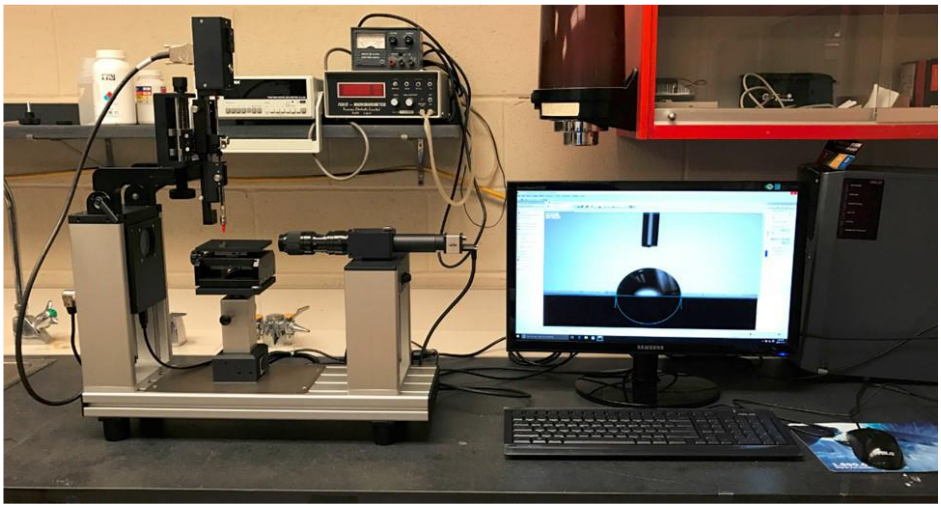

Figure 6. The Dataphysics OCA 15EC Contact Angle Measurement System [65].

3.6. Microstructure characterization

The fabricated surfaces were imaged with an FEI MLA 650F scanning electron microscope (SEM) (shown Figure 7a) using secondary electron imaging (SEI) mode to investigate the topography of the bare and coated surfaces. Secondary electrons that generally have less than 50 eV are detecting by the SE detector. This energy range limits the depth from within the specimen which the electron can escape. Therefore, the surface topography that secondary electrons detected is only a few nanometers. In the secondary electron image, the brightness at different positions is

associated with the number of secondary electrons detected by the SE detector. However, a flat surface will not release the secondary electrons from the surface due to the relatively small interaction volume. Edges provide greater amounts of surface area for low energy secondary electrons to escape. Thus, more secondary electrons are emitted, resulting in sharp areas appear brighter in the image. As the surface is more tilted or more surface features exist on the surface, more secondary electrons can be reached to the SE detectors, which results in a brighter image as compared to a flat surface. Therefore, the brightness in secondary images is ascribed to the topography of the surface.

The chemical composition data were collected using a high throughput Bruker energy dispersive X-ray (EDX) analytical system. The EDX characterization is an analytical method employed for the elemental analysis or chemical characterization of a metals, relying on an interaction of the electron beam, some source of X-ray excitation, and the sample. X-rays are generated when an electron from an inner shell is ionized and excited, and the electron from an outer shell fills to release energy. The energy difference between the higher-energy shell and the lower energy shell can be released in the form of an X-ray. These X-rays are material characteristics and usually used for elemental analysis.

Phase characterization of the electrodeposited samples was performed using a Rigaku Ultimate IV X-ray diffraction (XRD) (Figure 7b) with Cu-Kα source at 40 kV and 44 mA over a diffraction angle range of 20°-90° with a step size of 0.02°. The X-ray diffraction method is based on the constructive interference of monochromatic X-rays with a crystalline metal. The generated X-rays by a cathode ray tube, filtered to provide monochromatic radiation, collimated to concentrate, and directed toward the sample's surface.

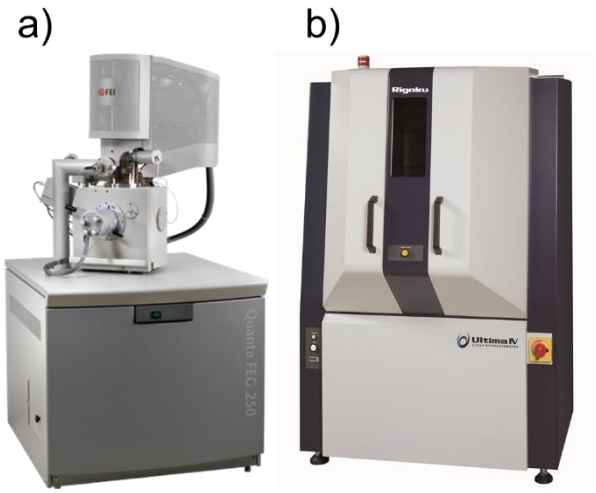

Figure 7. a) an FEI MLA 650F scanning electron microscope, b) Rigaku Ultimate IV X-ray diffraction

3.7. Cyclic Potentiodynamic Polarization (CPP) testing

To investigate the corrosion behavior and adhesion durability of the coating, cyclic polarization measurements of all fabricated surfaces were conducted utilizing an IVIUM CompactStat™ Potentiostat with a three-electrode cell setup based on the ASTM G5 standard for potentiodynamic polarization measurements (as shown in the Figure 8), using a graphite rod as the counter electrode (CE), a saturated silver/silver chloride (Ag/AgCl) as the reference electrode (RE), and the sample as the working electrode (WE) [66]. The samples were immersed in an aerated 3.5 wt. % NaCl solution to simulate seawater corrosion conditions at 25±0.5 °C using a temperature-controlled water bath. Before the tests, the open circuit potential (OCP) was monitored for 1 h for stabilization. For testing repeatability and obtain reliable average values, at least three samples were tested for each condition. Following the CPP testing, the corrosion morphology of the samples was investigated using the SEM.

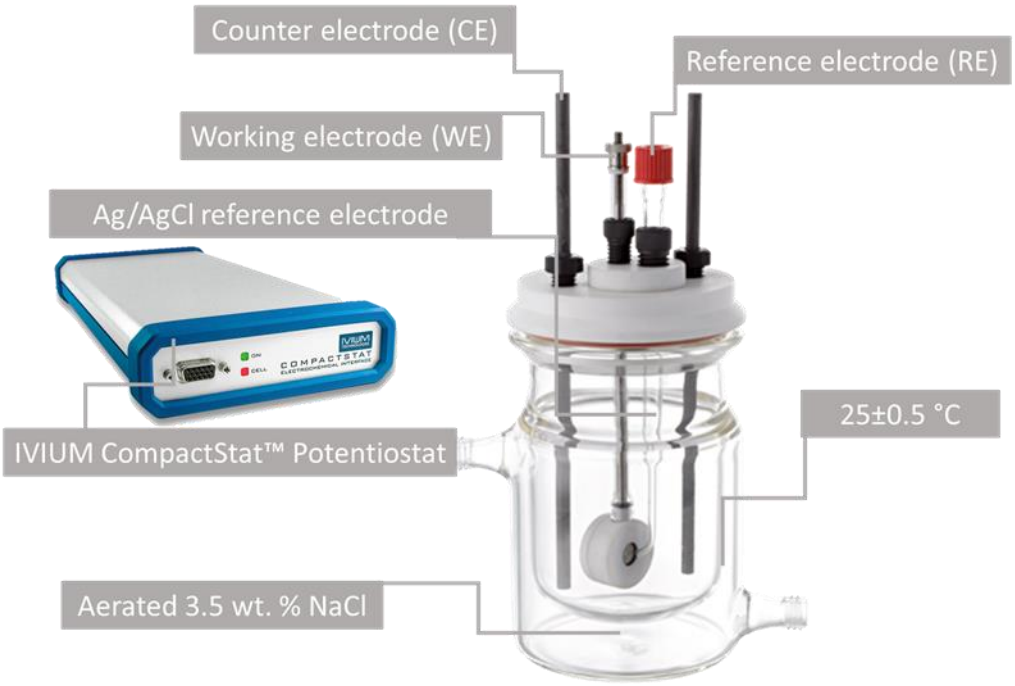

Figure 8. The schematic of Cyclic Potentiodynamic Polarization (CPP) testing setup.

3.8. Electrochemical Impedance Spectroscopy (EIS) analysis

To further investigate the coating adhesion over time, EIS tests were carried out on all samples in aerated 3.5 wt. % NaCl solution at 25±0.5 °C. Signals with ±0.01 V amplitude over the OCP with a frequency range between 100 kHz and 10-2 Hz with ten points per decade were applied. Before running each EIS test, the OCP was recorded for 1 h. Likewise, the repeatability of the EIS test results was measured by testing at least three samples.

3.9. Salt spray corrosion testing

The salt spray exposure testing is a standardized method to characterize the adhesion durability of the coatings on solid substrates [67]. The applied stress on the exposed coated surfaces during salt spraying can create surface erosion, causing more accelerated degradation of the applied coating as compared to the immersion testing in the same electrolyte. The test was

conducted by spraying atomized 3.5 wt.% NaCl solution at the pressure of 20 psi on the coated stainless steel samples inside the Ascott salt spray chamber (shown in Figure 9) at the room temperature and humidity level of 100%. Various exposure times, i.e. 24 h, 72 h, and 120 h, were adopted to evaluate the adhesion durability of the coatings. The NaCl droplets were accumulated on the coated surfaces and resulted in the formation of the so-called white rust [68]. After the completion of each test, the formed white rust and other corrosion products were chemically removed from the samples' surfaces, followed by ultrasonically cleaning of the samples in acetone. The tested samples were then dried in warm air for further CPP testing or SEM analysis.

Figure 9. Ascott salt spray corrosion test chambers

CHAPTER 4

4. Fabrication of super-hydrophobic 17-4 PH stainless steel surfaces through different surface treatment methods coupled with applying a super-hydrophobic coating

4.1. Summary

In this chapter, various micron and sub-micron scale finished surfaces followed by applying a low surface energy coating were employed to fabricate hydrophobic and super-hydrophobic surfaces on 17-4 PH stainless steel base material. The ground and polished surfaces of the base material were coated by applying a 30-50 µm thick super-hydrophobic dip coating, resulting in the average surface roughness (Ra) of ~ 0.03 µm and 0.02 µm, and steady-state contact angles of up to 152° and 146°, respectively, while the as-received coated base metal exhibited a contact angle of 140°. The electrochemical measurements in aerated 3.5 wt.% NaCl electrolyte revealed that the water-repelling property of the fabricated surfaces contributes to the anti-corrosion capability of the substrates. The corrosion testing results indicated that the lowest corrosion current density, highest corrosion potential, and highest pitting potential were measured for the coated ground surface followed by the coated polished surface. The electrochemical impedance spectroscopy (EIS) results also highlighted the significantly greater absolute value of impedance at lower frequency ranges for the coated ground and coated polished surfaces even after 240 h of immersion time in the electrolyte than the other fabricated surfaces.

4.2. Methodology

4.2.1. Material

Plates of martensitic type 17-4 PH stainless steel (SS) with nominal chemical composition of 16.70±0.05 wt.% Cr, 3.70±0.06 wt.% Ni, 2.91±0.07 wt.% Cu, Si and Mn ≤ 0.80 wt.%, and balance Fe were used in this study. The samples with the size of 6 mm thick × 8 mm wide × 50 mm long were prepared from the as-received material and used as the substrate material. The microstructure of the base material employed herein has been shown in our previous study to be composed of parallel laths of martensite and a low volume fraction of δ-ferrite [4].

4.2.2. Fabrication of Hydrophobic Surfaces

To prepare the hydrophobic and super-hydrophobic surfaces at different levels of surface roughness, the surface of the base metal was subjected to various surface finishing procedures, including mechanical grinding using 500 grit SiC abrasive paper (provided the ground surface finish), final polishing using a 0.02 μm alumina suspension (provided the polished surfaces), and sandblasting utilizing aluminum oxide abrasive particle as the blasting media with the particle size of 45-140 mesh size (provided sandblasted surfaces). To remove any contaminants from the samples' surfaces prior to and after any surface treatment, the samples were cleaned ultrasonically in acetone and dried in air. Following this step and after fabrication of the ground, polished, and sandblasted surfaces, all samples, including the cleaned base metal with no pre-treatment (provided the base metal sample), were coated by applying 30-50 μm thick commercially available low-energy super-hydrophobic dip coating (FluoroThane WT) [12]. The cleaned samples' surfaces were immersed in the super-hydrophobic coating solution for 60 s, followed by removing the samples from the solution at a steady rate to ensure uniform coverage of the surface, and then dried

in air. The coated samples were referred to as the coated ground (CG), coated polished (CP), coated sandblasted (CSB), and coated base metal (CBM) samples.

4.3. Results and Discussion

4.3.1. Super-hydrophobic Coating

The coating coverage on the surface was found to expand by increasing the immersion time. When the immersion time was less than 10 s, the surface coverage of the coating was not sufficient, creating a coating on the surface that was not visually detectable. The entire coverage of the surface was obtained when the immersion time was approximately 50 s. At longer immersion times (> 50 s), more evenly coated surfaces were obtained. The uniformity of the applied coatings on the surface was investigated using the SEM. Figure 10 shows the cross-sectional overview of the sample with the applied coating. As depicted by the white arrows in Figure 10, the measured thickness of the coating on the ground surface was about 45±5 µm. As evident from the SEM micrograph in Figure 10, the applied coating possesses a uniform thickness on the surface.

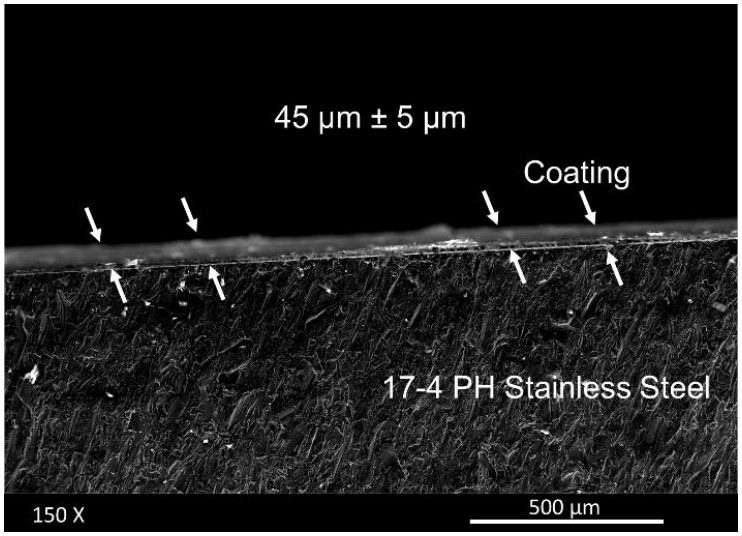

Figure 10. The SEM micrograph of the flu super-hydrophobic coating on the ground surface (CG).

4.3.2. Surface roughness measurement

Figure 11 presents the profilometer scans taken from different fabricated surfaces in this study. There are various roughness parameters capable of describing the surface roughness of a material. Among them, the R_a value, which is the arithmetic average of the absolute values of the profile heights over the mean line, is the most commonly used one. Mean line is the reference base-line about which the profile variations are averaged. The base-line of the roughness profile is usually indicated by either analog or digital filters, which is selected based on the roughness measurement line on the sample, using the equation 1 [69]:

$$R_a = \frac{1}{n}\sum|y_i| \qquad (i = 1 - n) \tag{1}$$

where R_a is the arithmetical mean deviation of the assessed profile over the base line for n different points over the scan line. The average roughness value (R_a) for the base metal was measured to be 5.52±0.120 μm. As expected, the R_a value is increasing from the polished surface (0.02±0.004 μm) to the ground (0.03±0.002 μm), and the sandblasted one (11.98±0.350 μm). It should be noted that after applying the super-hydrophobic coating on the base metal and the sandblasted surfaces, the surfaces' R_a values were not altered noticeably, whilst the coated ground and coated polished surfaces revealed an increased surface roughness to about 0.05 μm. The increased R_a value for the coated polished and ground surfaces is correlated to the inherent surface roughness of the hydrophobic coating, evenly covering the surface (see Figure 10), and as depicted in Figures. 11c and 11d, created a higher superficial roughness than that of the substrate.

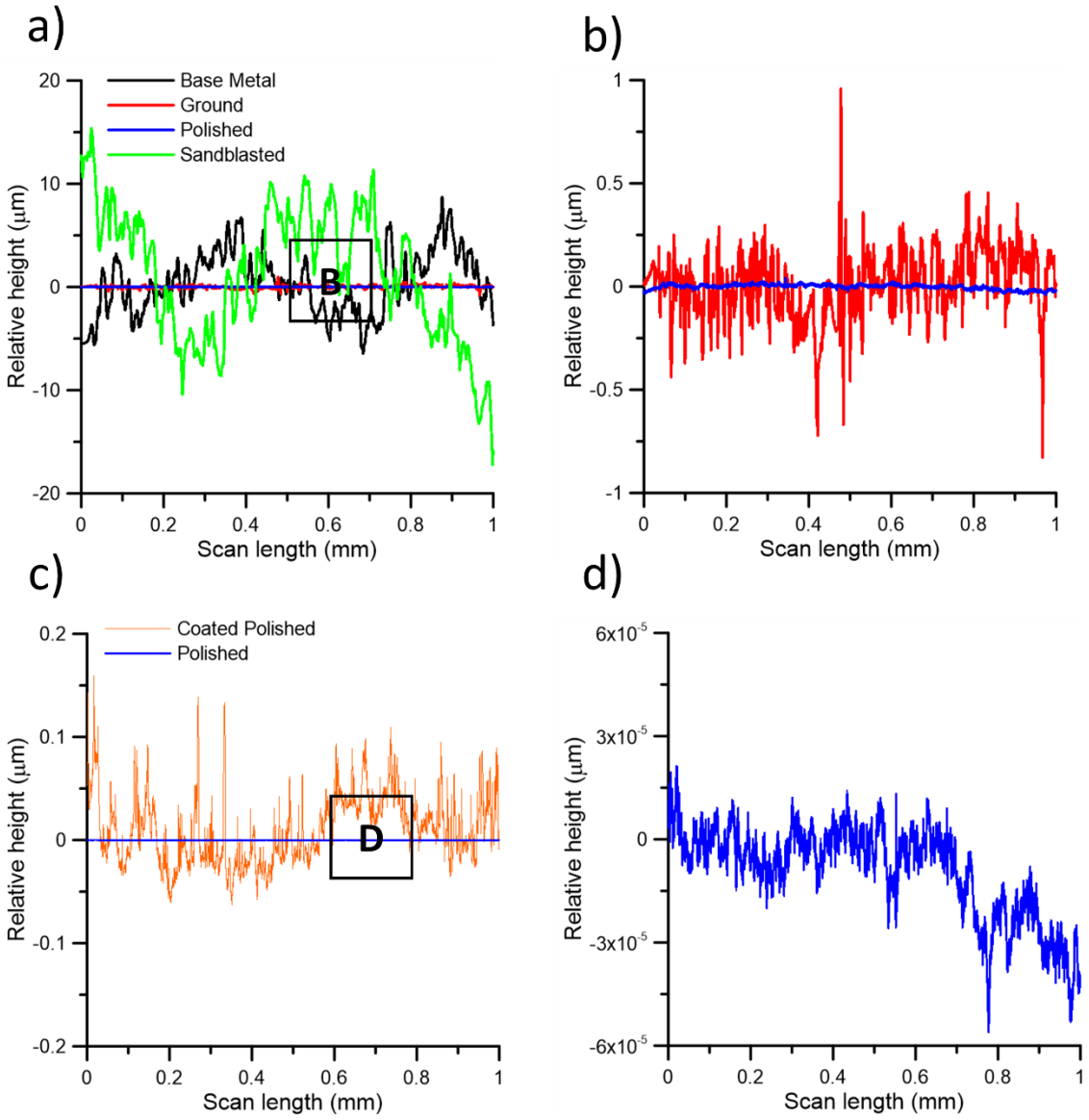

Figure 11. a) Representative profilometer scans of the base metal with no coating (black), ground (red), polished (blue), and sandblasted (green) surfaces; b) higher magnification of the enclosed area in (a) shown by B, c) surface profile of the coated polished (blue) surfaces, and d) higher magnification of the enclosed area in (c) shown by D.

4.3.3. Wetting Behavior

To quantify the surface wettability of the samples, the distilled water droplets' contact angles were measured on all coated and non-coated surfaces. The fabricated superficial roughness herein was expected to act as air-trapper features, leading to a reduced contact area between the liquid and the sample's surface. The contact angle of the fabricated surfaces can be interpreted using the classic analytical model of Cassie–Baxter, in which there is an assumption that droplets do not completely wet the rough surfaces due to the existing air pockets that are retained inside the surface roughness feature [70]. In this model, the apparent contact angle (θ_r^C) is measured by equation 2 [70]:

$$\cos\theta_r^C = f(\cos\theta_e + 1) - 1 \quad (2)$$

where θ_e is the intrinsic contact angle of a smooth surface and f is the liquid contact area fraction (the other fraction is the trapped air contact area). Applying the Cassie–Baxter model to both hydrophobic and hydrophilic surfaces shows that the contact angle on rough surfaces is higher than that of smooth surfaces, confirming the validity of the Cassie-Baxter model in this study.

The measured static contact angles for all fabricated surfaces before and after coating in this study are shown in Figure 12. The wettability of the coated surfaces was found to vary with the surface roughness. As expected, the bare base metal with no coating revealed the lowest contact angle of 74°±3°. After applying the hydrophobic coating on the base metal, its contact angle increased drastically to 140°±2°, although in the hydrophobic range, still below the minimum contact angle required for a super-hydrophobic surface (150°) [4]. Contact angle measurements before and after coating were also performed to investigate the impact of applying the super-hydrophobic coating on wettability of the fabricated surfaces having different surface roughness. As indicated from the presented data in Figure 12, albeit the coating itself is reported to be super-

hydrophobic by its nature [63], the higher superficial roughness of the base metal and the sandblasted surfaces has adversely affected the super-hydrophobicity function of the coating layer and resulted in contact angles lower than 150° for the coated base metal and coated sandblasted surfaces. On the other hand, the more smoothed polished, and in particular the ground surface, illustrated a near super-hydrophobic behavior with contact angle values of 146° and 152°, respectively. Therefore, based on the contact angle data, both the fabricated submicron roughness and application of the super-hydrophobic coating on the coated ground/polished surfaces, have contributed to the super-hydrophobic property of the surface. In addition, the fabricated surface roughness on the ground surface seems to be more effective than that of the polished surface in lowering the wettability and improving water repellency property of the coated surface, leading to the highest contact angle for the coated ground surface. Previous studies have also reported an analogous behavior for a ground surface finished carbon steel than its polished counterpart [71].

Interestingly, a similar trend was detected in the contact angle variation of the samples before and after applying the hydrophobic coating, confirming that the surface roughness would retain its impact on the wettability of the samples, regardless of the existence of the coating layer on the samples' surfaces. It is well established that a properly fabricated surface roughness can contribute to the improved hydrophobicity of the surface through maintaining the air pockets between the substrate and the liquid on the surface [3], [4].

The coating has further modified the contact angles by decreasing the surface energy of each sample. Therefore, in the case of coated polished and ground surfaces, by combining the impact of having optimum sub-micron size features (creating the surface roughness (R_a) of 0.02, and 0.03 µm, respectively, as shown in Figure 11) and applying a super-hydrophobic coating with R_a value of 0.05 µm, near to super-hydrophobic surfaces can be fabricated with the contact angles of

146°±4° and 152°±2°, respectively (Figure 12). On the other hand, if the surface roughness is not in a proper size, such as the roughness of the as-received base metal and sandblasted samples with R_a values 5.52 µm and 11.98 µm, respectively, even applying the super-hydrophobic coating on such surfaces does not contribute to a super-hydrophobic property. Consequently, the base metal and sandblasted surfaces both revealed only hydrophobic surfaces with contact angles of 140°±2°, and 138°±3°, respectively.

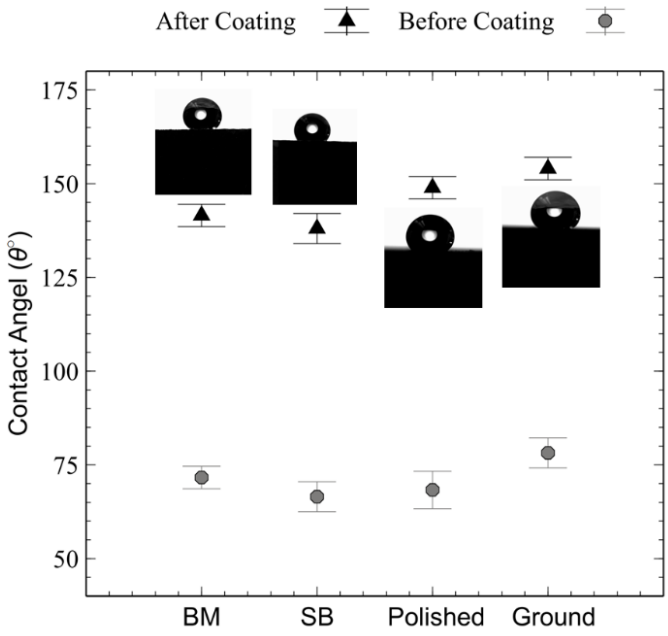

Figure 12. Effect of applying the super-hydrophobic coating on static contact angles of the base metal (BM), sandblasted (SB), polished, and ground surfaces.

4.3.4. Corrosion Behavior

Accelerated electrochemical testing is generally considered as a reliable and practical method to investigate the corrosion resistivity and electrochemical stability of metals [72]. Figure 13 shows the cyclic polarization results of all fabricated coated samples as compared to that of the base metal. The corrosion current density (I_{corr}) of all samples were found to be lower than 1.4

μAcm^{-2}, indicating the high corrosion resistivity of this grade of stainless steel in a simulated marine environment, which is in agreement with previous studies [4], [73]. Also, Table I summarizes the electrochemical properties obtained and calculated from the cyclic polarization plots shown in Figure 13. As a general trend, a better corrosion resistance is evidenced by an increase in the corrosion potential and a decrease in the corrosion current density. Therefore, according to the polarization graphs, the coated ground and coated polished surfaces revealed a higher corrosion resistance than the other surfaces, with corrosion potentials of 0.092 $V_{Ag/AgCl}$ and -0.051 $V_{Ag/AgCl}$, and corrosion current densities of 3.433×10^{-3} μAcm^{-2} and 6.172×10^{-3} μAcm^{-2}, respectively. Furthermore, the polarization graphs revealed the typical passive-active transition behavior of the materials (passive film breakdown potential, also known as the pitting potential (E_{pit})) at potentials of approximately 348 $mV_{Ag/AgCl}$ and 710 $mV_{Ag/AgCl}$ for the coated polished and coated ground samples, respectively. It should be noted that the passive window range of the polished and ground surfaces ($E_{corr.}$+200 $mV_{Ag/AgCl}$ and $E_{corr.}$+500 $mV_{Ag/AgCl}$, respectively) were noticeably higher than the other surfaces. Also, according to the polarization data given in Table I, the polarization resistance (R_p) of the coated polished and ground surfaces were 1.100×10^{7} $\Omega.cm^2$ and 1.375×10^{7} $\Omega.cm^2$, respectively, and significantly higher than the other roughened surfaces. These electrochemical properties suggest the improved corrosion resistance of the coated ground and coated polished samples than the other fabricated surfaces against both uniform and localized corrosion attacks.

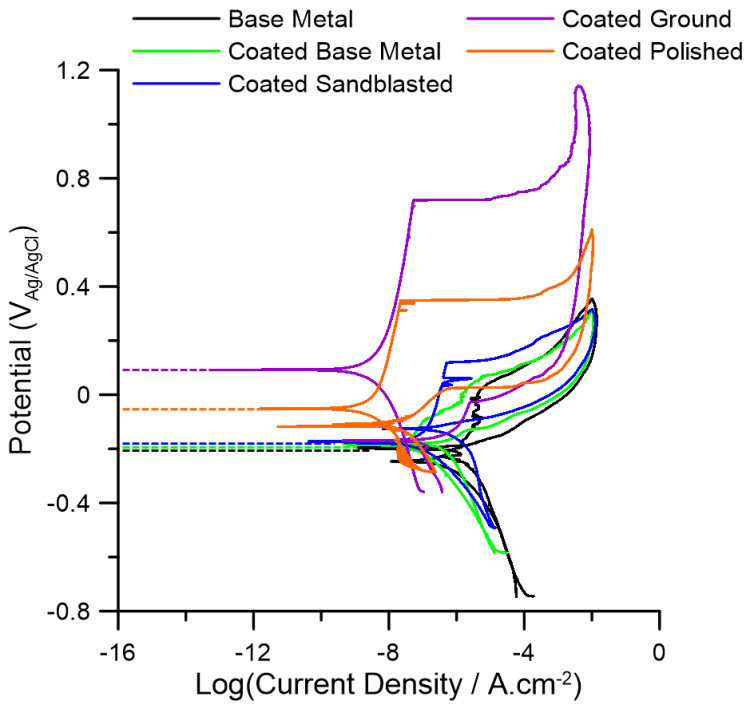

Figure 13. Cyclic polarization plots of the base metal (BM), coated base metal (CBM), coated sandblasted (CSB), coated polished (CP), and coated ground (CG).

Table 1. Polarization parameters deducted from the cyclic polarization plots shown in Figure 13.

Surface	R_p ($\Omega.cm^2$)	$E_{Corr.}$ ($V_{Ag/AgCl}$)	E_{pit} ($V_{Ag/AgCl}$)	$I_{Corr.}$ (μAcm^{-2})
CG	1.375×10^{7}	0.092	0.710	3.433×10^{-3}
CP	1.100×10^{7}	-0.051	0.348	6.172×10^{-3}
CSB	1.073×10^{5}	-0.174	0.118	9.519×10^{-2}
CBM	1.525×10^{6}	-0.178	0.002	4.449×10^{-2}
BM	4.893×10^{4}	-0.245	0.001	1.387

The substantial improvement in corrosion resistance of the coated ground and coated polished surfaces can be ascribed to their enhanced hydrophobicity and water repellency properties through fabrication of an optimum sized surface roughness along with applying the super-hydrophobic coating on their surfaces. The coated base metal and sandblasted surfaces revealed significantly

lower corrosion resistance than the coated polished and ground surfaces. This was confirmed by noticeably lower pitting potential of the surface (early break down of the passive film) at around 100 $mV_{Ag/AgCl}$. Hence, the super-hydrophobicity of the surfaces positively impacts the corrosion properties of the 17-4 PH stainless steel substrate. It is worth mentioning that the base metal with no coating showed the lowest (most negative) corrosion potential and the lowest passivation resistance (E_{pit}), indicating its greater corrosion tendency among others, which is another compelling evidence for the contribution of the super-hydrophobic and hydrophobic properties on the electrochemical stability of the samples.

Likewise, the corrosion current density (I_{corr}) of the coated base metal and the coated sandblasted 17-4 PH SS were found to be at least one order of magnitude higher than that of the coated polished and coated ground surfaces, which is consistent with the improved corrosion resistance of the coated ground and polished samples. Therefore, the surface roughness and its resultant water-repellency property were found to further contribute to better corrosion properties of the 17-4 PH SS surfaces.

Beside higher pitting potential and lower corrosion current density in the coated ground and polished surfaces, the pitting of these surfaces was not detected even after a long immersion time in seawater simulated solution. Figure 14 shows the corrosion morphology of the coated as-received base metal and coated ground surfaces after cyclic polarization test, followed by removing the corrosion products. As clearly depicted from Figures. 14c and 14d, corrosion pits were not detected on the corroded surface of the coated ground sample, while the coated base metal indicated pits formation on the entire corroded surface after cyclic polarization test (shown by arrows at a higher magnification in Figure 14b). The coated polished surfaces also revealed a minor corrosion attack with similar morphology to the coated ground surface. Therefore, the corrosion

morphology of all fabricated surfaces was found to be consistent with the polarization behavior of the samples (Figure 13), revealing a more severe pitting corrosion attack on the base metal and coated base metal and coated sandblasted surfaces, as opposed to the coated ground and polished surfaces with a lower tendency to pitting in a simulated marine environment.

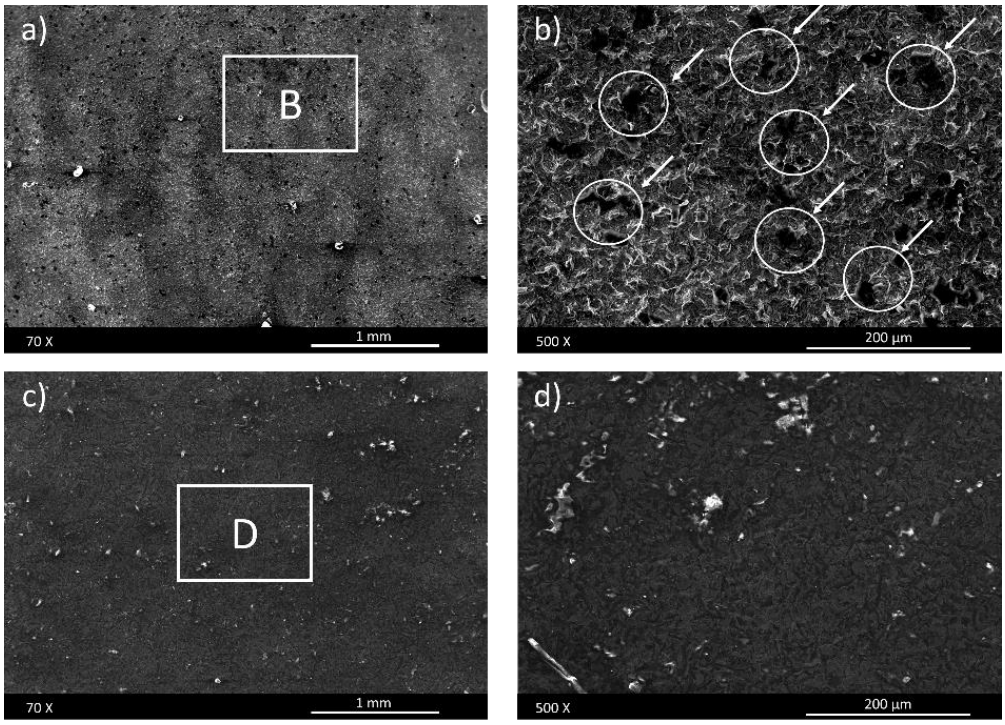

Figure 14. SEM micrographs of the a) base metal (BM), b) higher magnification of the enclosed area in (a) shown by B, c) coated ground (CG) surface, and d) higher magnification of the enclosed area in (c) shown by D, after CP testing followed by corrosion product Removal

All in all, the corrosion behavior of the fabricated surfaces herein can be rationalized by considering the concomitant effects of the surface roughness and super-hydrophobicity of the surfaces. Among all these factors, surface roughness has a prominent influence on the corrosion resistance of the samples [74]. As a general trend, it is known that a smoother surface finish gives rise to a better corrosion resistance properties, as the superficial roughness would lead to a drop in

the electron work function and increase the corrosion rate [75]. Surface deformation, density of superficial defects, and the formed micro-strain in the material's surface layers resulted from the fabrication process have been reported to deteriorate the pitting resistivity of the steels [76]. Analogously, in the sandblasted sample, because of the formation of localized deformed areas on the surface resulted from the impact of the blasting media to the surface, the dislocation density in the surface layers is increased. The increased dislocation density in the material's surface layers leads to the formation of a large number of active sites susceptible to the corrosion attack when exposed to a corrosive electrolyte [75].

In the context of the hydrophobicity impact on the corrosion behavior of the surface, it should be noted that an optimized surface roughness can create a super-hydrophobic surface, which in turn can contribute to an enhanced corrosion property [4]. As a conclusion, according to the Cassie-Baxter model, the coated ground surface with its optimum surface roughness with R_a value of 0.03 µm can retain the entrapped air within its interstices more adequately than the other surfaces with either lower surface roughness, such as the coated polished surface with the roughness of 0.02 µm, or higher surface roughness, such as the as-received and sandblasted surfaces with the R_a values of 5.52 µm and 11.98 µm, respectively.

Figure 15 shows the modification of the EIS spectra for various immersion times in the aerated 3.5 wt.% NaCl solution up to 240 h of immersion time. Before the EIS test, the samples were immersed in the electrolyte solution for 1 h at OCP to ensure a steady state behavior was attained.

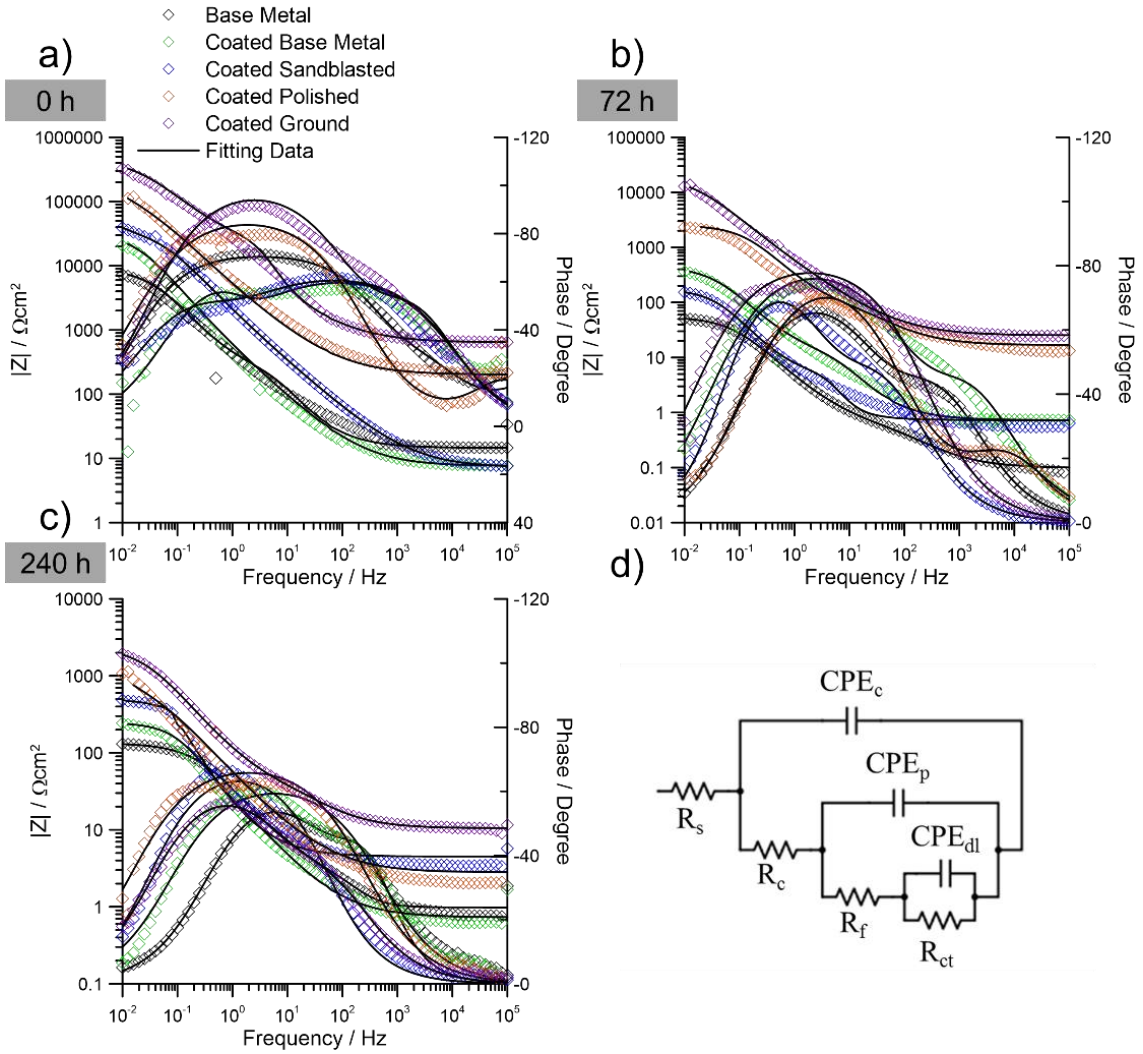

Figure 15. The EIS spectra and the fitting data of the base metal and the fabricated hydrophobic surfaces in aerated 3.5 wt.% NaCl solution after a) 0 h, b) 72 h, c) 240 h, and d) the proposed equivalent circuit.

At the initial immersion time (0 h), the EIS results show a capacitive response with a wide frequency range, indicating the existence of a stable passive film and the coating layer on the samples' surfaces. Comparing the peaks of the phase angle plots of all samples reveals that the coated polished and coated ground samples have a higher maximum phase angle values (more negative) at lower frequency ranges, suggesting the greater stability of the barrier layer on these

samples, comprised of the coating and the passive film. These layers act as barriers between the stainless steel substrate and the corrosive electrolyte, and protect the base metal from anodic dissolution in the electrolyte. Differently, the coated base metal and coated sandblasted samples showed two small capacitive loops. This indicates that the corrosive medium has penetrated to the coating-base metal interface, causing the charge transfer to be the controlling factor in corrosion. Furthermore, as a general trend, the continuous absorption of the corrosive species, such as chloride ions, into the coating thickness has diminished the overall protective nature of the applied coating [77], as evidenced by the observed reduction in the capacitive peaks at longer immersion times.

Analogously, the Bode plots in Figure 15 present a significantly higher impedance (|Z|) values at lower frequency ranges for the coated ground and coated polished surfaces than the other fabricated surfaces over the entire immersion times. This is attributed to not only the existence of a stable passive layer and the coating on the surface, but also the water repellency nature of the fabricated super-hydrophobic 17-4 PH stainless steel surfaces. The absolute values of impedance for the fabricated coated ground surface at lower frequencies (0.01 Hz) even after 240 h of immersion time is higher than 2000 Ωcm^2, confirming the high corrosion resistance of the fabricated surfaces owning super-hydrophobic property. In contrast, the as-received base metal and the coated sandblasted surfaces revealed drastically lower absolute values of impedance than the other surfaces (shown in Figure 15c), attributed to their lower corrosion resistance. This behavior can be ascribed to the cathodic destabilization of the passive film on as-received and sandblasted 17-4 stainless steel surfaces due to their surface roughness and inadequate super-hydrophobicity property as compared to the coated ground and coated polished surfaces [72]. Therefore, the obtained EIS results are in agreement with the results of the cyclic polarization tests

(Figure 13) and aligned with the measured contact angle data (Figure 12), meaning the coated ground and coated polished samples possessing a near super-hydrophobic surface revealed a better corrosion performance in a simulated seawater environment.

To further rationalize the pitting corrosion of the fabricated samples, the equivalent electrical circuit (EEC) model shown in Figure 15d was used and fitted to the experimental EIS data. It is assumed that the corrosive species can reach to the coating/base metal interface through the coating porosities even after 1 h of immersion time, provoking the charge transfer as the dominant factor in controlling the corrosion reactions [77]. Therefore, the adopted EEC characterizes not only the coating stability and the formed passive film's electrical properties, but also the charge transfer on the base metal surface. This simplified circuit uses three *RQ* elements, which leads to an equivalent model of $R_s+Q_c\times(R_c+Q_p\times(Q_{dl}\times R_{ct})+R_f))$ (see Figure 15d). In this model, R_s describes the solution resistance, R_c and CPE_c correspond to the resistance and the constant phase element of the applied coating layer (assuming that the coating has a porous nature on the substrate surface), respectively, R_f and CPE_p present the resistance and the constant phase element of the passive layer, respectively, R_{ct} is the charge transfer resistance (corroding pit resistance) and the respective constant phase element CPE_{dl} refers to the double layer (*dl*) charging-discharging at the alloy's surface. The use of constant phase element (*CPE*) instead of capacitor can be justified based on non-ideal capacitive behavior of heterogeneous interfaces herein. The superficial roughness on the fabricated samples is one of the factors that creates heterogeneities along the interfaces and contributes to this non-ideal behavior [78].

Based on the equivalent electrical circuit model, a higher R_f (passive film resistance) value indicates a higher resistance against the penetrating corrosion species, such as chloride ions. The charge transfer resistance or pitting resistance (R_{ct} element) can be considered as a major factor

that influences the corrosion resistance of the metal in such a corrosive environment [79]. The EIS results can also be employed to investigate the coatings' durability on the surface when exposed to the corrosive electrolyte solution. The coating resistance (R_c) could represent the anti-penetrating ability of the coating, and the CPE_c can similarly relate to the diffusion behavior of electrolyte solution into the coating, corresponding to the anti-durability of the coating [80].

The calculated fitted parameters of the proposed EEC herein from the EIS graphs are summarized in Table II. The critical parameter that describes corrosion behavior of 17-4 PH stainless steel using EIS is the charge transfer resistance, R_{ct} [78]. The higher the charge transfer resistance (R_{ct}) value, the better the corrosion resistivity of the surface against localized pitting is. The charge transfer resistance of 17-4PH stainless steel for the coated ground and coated polished surfaces were calculated to be significantly higher than that of other fabricated surfaces. This is consistent with the cyclic polarization results in Figure 13. Accordingly, the coated ground and coated polished samples have much better corrosion resistance than other surfaces in a simulated seawater solution. Moreover, the EIS results revealed that the coatings resistance (R_c) of all coated samples gradually decreased, while their CPE_c values gradually increased by increasing the immersion time. However, the coated ground and coated polished samples exhibited the highest R_c and the lowest CPE_c, confirming the best corrosion protection properties of the applied coating on those surfaces [77].

Table 2. The EIS parameters of the equivalent circuit shown in Figure 15.

Time (h)	R_s ($\Omega.cm^2$)	R_c ($\Omega.cm^2$)	R_f ($\Omega.cm^2$)	R_{ct} ($\Omega.cm^2$)	CPE_c ($\mu S\ s^n\ cm^{-2}$)	CPE_p ($\mu S\ s^n\ cm^{-2}$)	CPE_{dl} ($\mu S\ s^n\ cm^{-2}$)
BM							
1	10.31	13.6	32.3	52.4	4.21	41.2	1.21×10^{3}
72	3.24	1.15	25.7	4.32	0.321	5.23×10^{-2}	4.04×10^{-3}
240	5.58	0.22	11.2	22.4	0.592	1.31×10^{-4}	3.25×10^{-5}
CBM							
1	9.24	12.23	73.1	92.1	4.53×10^{-3}	4.23×10^{2}	5.14×10^{2}
72	10.23	2.87	1.24	8.87	4.19×10^{-3}	2.21×10^{-2}	3.56×10^{-3}
240	8.23	0.356	14.2	1.98	3.27×10^{3}	0.221	4.23×10^{2}
CSB							
1	14.23	64.4	2.33	3.89×10^{2}	2.45×10^{3}	3.29×10^{-5}	1.54×10^{-4}
72	3.24	2.32	2.87	54.3	1.04×10^{-2}	9.23×10^{-4}	6.33×10^{-2}
240	15.67	1.07	0.356	9.29	5.04×10^{2}	4.14×10^{2}	9.34×10^{-4}
CG							
1	12.09	2.13×10^{2}	30.2	5.36×10^{3}	1.43×10^{-6}	2.03×10^{3}	8.12×10^{3}
72	6.87	1.20×10^{2}	23.4	3.22×10^{3}	2.05×10^{-3}	4.23×10^{3}	4.35×10^{2}
240	8.43	2.24	10.6	1.89×10^{2}	1.34×10^{-4}	1.74×10^{2}	1.98×10^{3}
CP							
1	4.56	89.4	92.4	9.76×10^{2}	3.03×10^{-5}	4.56×10^{2}	6.77×10^{-4}
72	16.34	72.5	14.0	2.04×10^{3}	9.32×10^{-4}	2.51×10^{2}	1.23×10^{3}
240	7.45	1.05	9.68	79.8	6.34×10^{-3}	64.4	3.34×10^{-2}

CHAPTER 5

5. The impacts of the substrate's surface roughness on the fabrication and durability of the developed Zn electrodeposited coating

5.1. Summary

In this chapter, super-hydrophobic 17-4 PH stainless steel surfaces were fabricated for applications in harsh marine environment. The impacts of the substrate's surface roughness on the fabrication and durability of the developed super-hydrophobic coating, comprised of a Zn electrodeposited layer capped with 0.05 M stearic acid, were investigated. Various micron and sub-micron scale finished surfaces with different surface roughness, namely as-received (Ra ~ 4.62 μm), sandblasted (Ra ~ 11.93 μm), and ground (Ra ~ 0.39 μm) surfaces, were fabricated, followed by applying Zn electrodeposited coating to improve the water-repellent properties of the stainless steel substrate. The cyclic potentiodynamic polarization and electrochemical impedance spectroscopy (EIS) results measured in aerated 3.5 wt.% NaCl electrolyte at room temperature along with salt spray testing highlighted a significantly better uniformity and adhesion durability of the coating on the as-received substrate correlated to its optimum surface roughness. The coated 17-4 PH stainless steel surfaces were found effective in preventing the aggressive chloride ions from approaching the substrate, leading to the improved corrosion performance of the material.

5.2. Methodology

Several surface finishing procedures were applied on the as-received 17-4 PH stainless steel plate to produce samples with different superficial roughness. These include mechanical grinding using 500 grit SiC abrasive paper (provided the ground surface finish) and sandblasting utilizing aluminum oxide abrasive particle as the blasting media with the particle size of 70-80 mesh size

(provided sandblasted surfaces). To remove any contaminants from the samples' surfaces prior to and after any surface treatment, the samples were cleaned ultrasonically in acetone and dried in air. The surface roughness of the fabricated samples was evaluated using a surface profilometer (Alpha-Step D-120 Stylus Profiler). Each surface was scanned employing the fine stylus with a 2 μm tip radius at the scanning speed of 0.01 mm/s and the scanning step size of 0.04 μm.

5.3. Results and Discussion

5.3.1. Surface roughness

The arithmetic average of the absolute values of the profile heights over the mean line (R_a) is the most common way of describing the surface roughness of materials [81]. The mean line is the line about which the variation of the height is averaged. The roughness profile baseline is shown by either analog or digital filters, which is selected based on the roughness measurement line on the sample. The R_a values for different fabricated surfaces are given in Table 1. As expected, R_a value is increasing from the ground surface to the as-received and the sandblasted one. Figure 16 shows the 2D surface roughness profiles of the roughened surfaces before and after applying the coating. As Figure 16a shows, the sandblasted surface has a high degree of surface irregularities as a result of the fabrication process, creating a superficial roughness of 11.93 ± 0.22 μm. However, the obtained roughness on the as-received and ground surfaces was noticeably lower than that of the sandblasted one. The measured roughness values for as-received and ground surfaces were 4.62 ± 0.15 μm and 0.39 ± 0.03 μm, respectively. This was found to be in agreement with the results reported in a previous study by the authors [5].

Moreover, it is worth mentioning that after applying the Zn electrodeposited coating, the surface roughness for all three surfaces is increased with the same trend (see Figure 16b), leading

to the coated sandblasted surface as the roughest surface (R_a = 23.38±0.21 µm) and the coated ground surface as the smoothest surface (R_a = 16.02±0.12 µm). The increased R_a value for the coated surfaces is correlated to the inherent surface roughness of the Zn electrodeposited coating, evenly covering the surface. Such variations in the surface roughness values is expected to affect the water-repellent properties of the surface drastically.

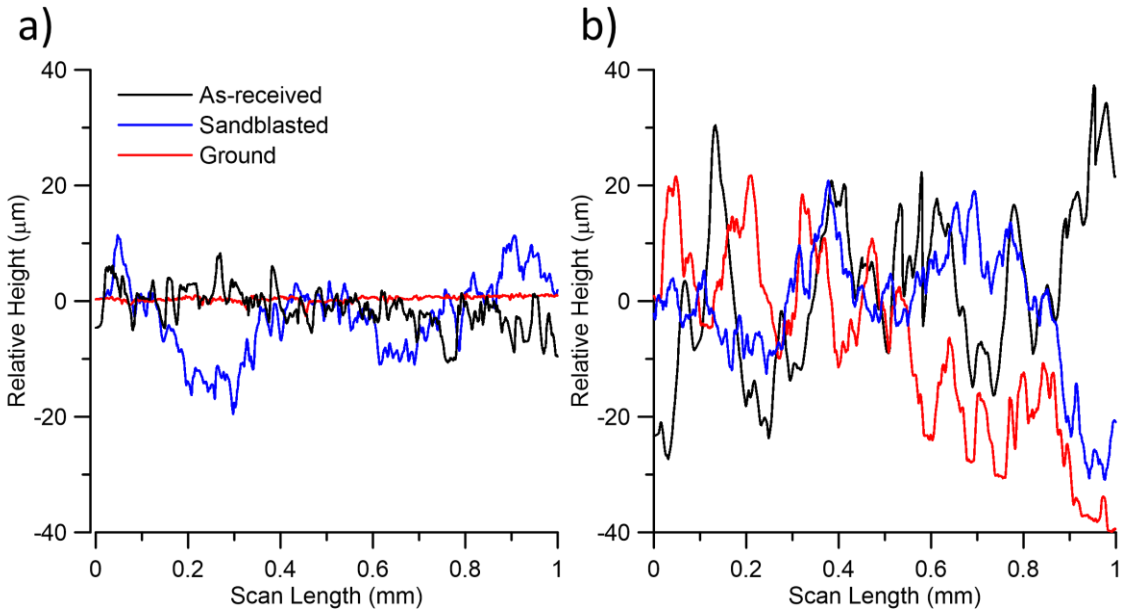

Figure 16. Representative profilometer scans of the as-received (black), ground (red), and sandblasted (blue) 17-4 PH stainless steel surfaces a) without coating and b) with electrodeposited Zn coating.

Table 3. The mean roughness (Ra) for different fabricated samples in this study.

Surfaces	Before Electrodeposition R_a (µm)	After Electrodeposition R_a (µm)
Ground	0.39±0.03	16.02±0.12
Sandblasted	11.93±0.22	23.38±0.21
As-received	4.62±0.15	19.89±0.51

5.3.2. XRD results

The XRD results taken from one of the coated samples is shown in Figure 17, confirming the formation of the Zn coating on the stainless steel substrate [7]. The diffraction peaks belong to both Zinc and the stainless steel substrate were detected on the spectra. The appearance of BCC-iron diffraction peaks on the XRD spectra indicates that the 17-4 PH stainless steel substrate is primarily composed of the ferrite phase. The d-spacing might have a slight discrepancy from the Joint Committee on Powder Diffraction Standards (JCPDS) card due to the several reasons such as sample height, the surface flatness of the sample, and residual surface stress.

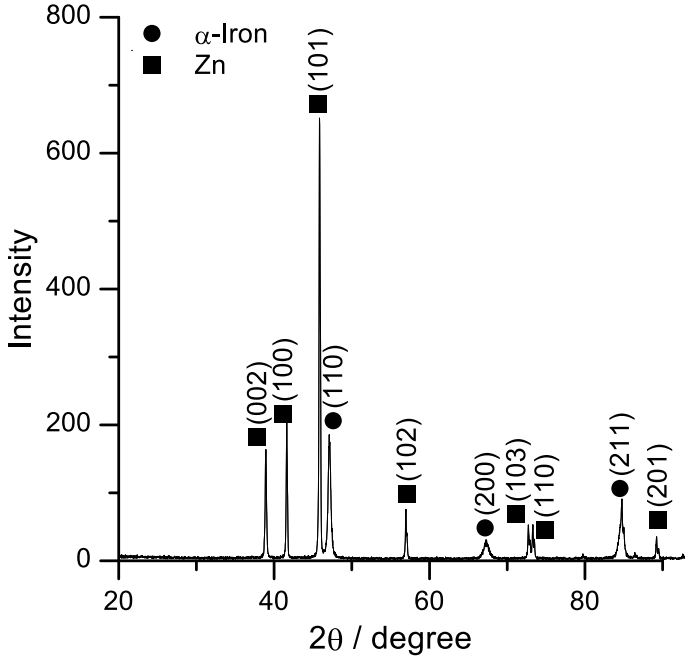

Figure 17. X-ray diffraction spectra of the Zn electrodeposited sample.

5.3.3. Wetting behavior

The water droplet contact angle measurements were performed to investigate the impact of applying the super-hydrophobic coating on the wettability of the fabricated surfaces having different surface roughness prior to applying the coating. All coated surfaces collectively revealed

a similar wetting behavior, characterized by a super-hydrophobic surface possessing an extremely low surface energy, causing the water droplet to roll off from the surface as soon as the droplet was dispensed on the surface. Figure 18 shows two steps during the contact angle measurements of the droplets on the coated as-received surface. A 5 μL water droplet was dispensed by a needle on the electrodeposited surface (Figure 18a). Once the droplet was detached from the needle, it rolled off from the surface instantaneously. Therefore, the static contact angle of the droplets on the coated samples was not possible to be measured. A video file recorded from the fabricated super-hydrophobic surfaces in this study is attached to the supplementary documents of this paper.

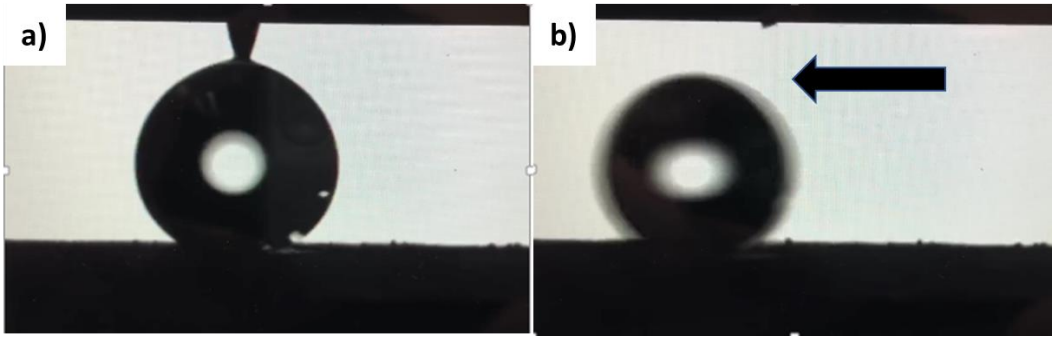

Figure 18. The water droplet images on the coated as-received 17-4 PH stainless steel substrate taken during the contact angle measurement, (a) a droplet placement on the surface and (b) the droplet rolling off the surface.

To check the coating morphology and its uniformity on the fabricated surfaces, scanning electron microscopy images were taken from different surfaces before (Figures. 19a-19c) and after (Figures. 19d-19f) coating. As Figures. 19a-19c show, the sandblasted sample revealed more surface irregularities than the ground surface or the as-received one, confirming the profilometer results shown in Figure 16. Moreover, the EDX concentration maps taken from the surface of the

coated samples after electrodeposition depict the correlation between the surface roughness and the uniformity of the coating coverage. As Figures. 19d-19f show, the as-received surface with the surface roughness of 4.62±0.15 µm demonstrates the best uniformity of the coating. On the other hand, the ground surface with the minimum surface roughness (0.39±0.03 µm) and sandblasted one with the maximum surface roughness (11.93±0.22 µm) show the non-uniform coverage of the Zn electrodeposited coating on the surface. Therefore, the compositional analysis of the coated surfaces confirmed that some degree of roughness on the surface contributes to the uniformity of the Zn electrodeposited layer on 17-4 PH stainless steel surface, resulting in the improved uniformity of the coating in the order of as-received > sandblasted > ground surfaces [81].

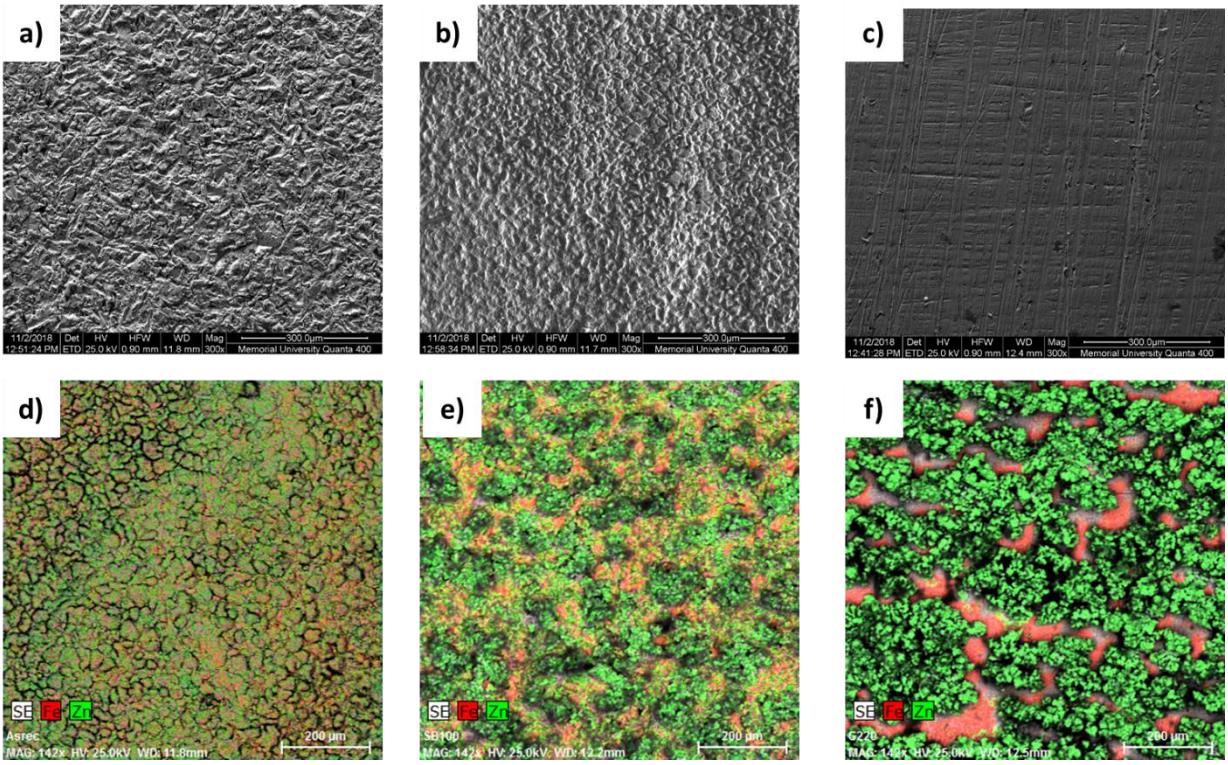

Figure 19. SEM micrographs taken from the surface of a) as-received, b) sand-blasted, and c) ground samples. The EDX chemical concentration maps superimposed on the SEM images of the coated d) as-received, e) sand-blasted, and f) ground surfaces.

To investigate the adhesion durability of the applied coatings in a harsh environment, the coated samples were immersed in aerated 3.5 wt.% NaCl solution at 25±0.5 °C for 24 h and 72 h, followed by measuring their wettability. Figure 20 shows the static contact angle values after different immersion times. As expected, the as-received sample with better uniformity of the coating coverage (shown in Figure 19d) showed the lowest contact angle reduction after 72 h of immersion, around 43°. However, the sandblasted and ground surfaces with the highest and lowest surface roughness and weaker coating quality compared with the as-received, show more reduction in the contact angles, ~ 73° and 84°, respectively. Surface roughness and contact angle measurements confirmed that albeit the coating itself created an optimum surface roughness and entirely covered the surface roughness of initial surfaces, the superficial roughness of the as-received surface has positively contributed to not only the uniformity of the Zn electrodeposited coating layer, but also its adhesion durability, resulted in the lowest contact angle reductions for the coated as-received surface after 24 h and 72 h of immersion time in seawater environment. On the other hand, the ground surface as the smoothest surface revealed the highest reduction in contact angle after 72 h of immersion. Therefore, based on the contact angle data, the fabricated submicron roughness before applying the super-hydrophobic coating on the 17-4 PH stainless steel surface has altered the adhesion durability of the super-hydrophobic coating significantly. Interestingly, the same trend for the static contact angles variations was detected after 24 h and 72 h of immersion time, confirming that the surface roughness would retain its impact on the coating durability on the surface even after long immersion time.

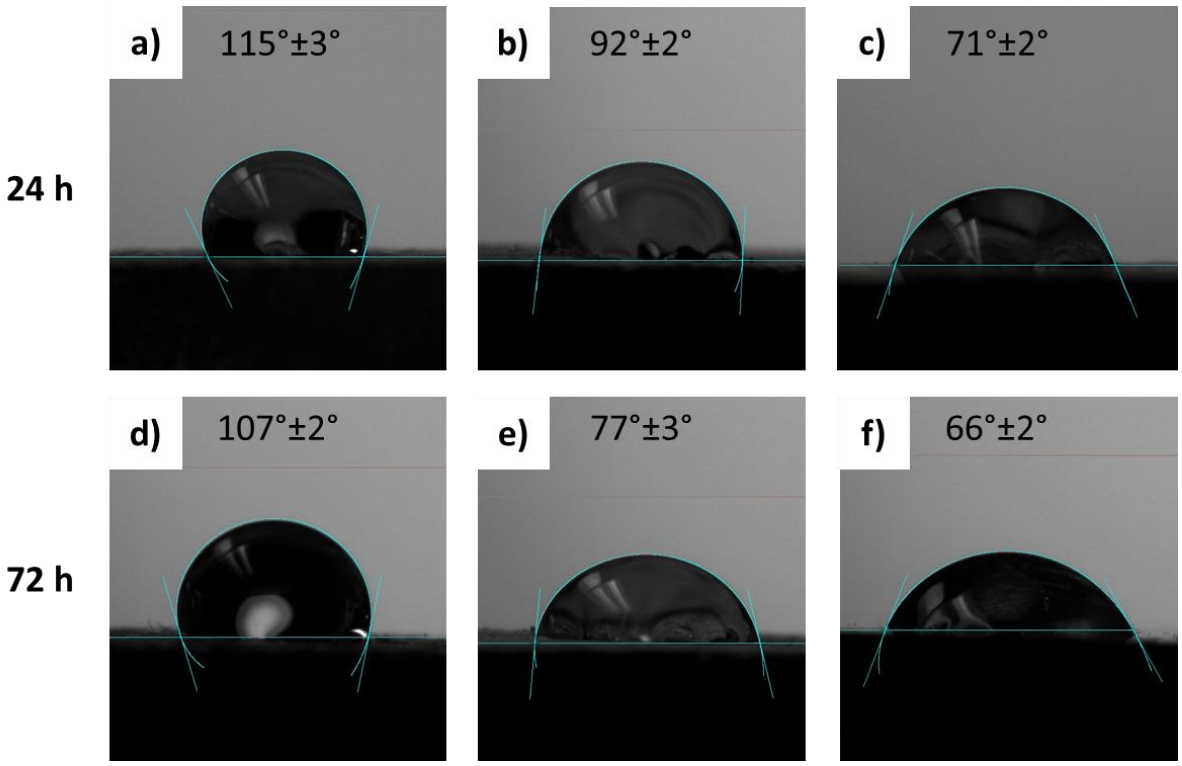

Figure 20. Contact angle measurements of the coated a) as-received, b) sand-blasted, c) ground after 24 h of immersion time, and d) as-received, e) sand-blasted, f) ground after 72 h of immersion time in an aerated 3.5 wt. % NaCl solution.

5.3.4. Coating Adhesion

In order to further study the adhesion durability of the applied coatings over time, the electrochemical impedance spectroscopic analysis of the fabricated samples in aerated 3.5 wt.% NaCl solution was performed. The resultant Bode and phase plots are as shown in Figure 21. After 1 h of immersion time (Figure 21a), the EIS spectrum of the bare as-received surface shows very high values ($>10^5$ Ωcm^2) of impedance modulus (|Z|) at the low-frequency limit, and its corresponding phase angle was close to -70 degree, affirming the high corrosion resistance properties of 17-4 PH stainless steel. Only one time constant could be detected on the impedance spectra, ascribing to the barrier characteristic of the passive film on the stainless steel. Differently,

the coated surfaces show significantly lower impedance values (in the range of 1000-2000 Ωcm^2). The drastically lower impedance of the coated samples is correlated to the electrochemically active nature of the electrodeposited Zn layer exposed to the electrolyte, meaning the measured impedances and phase angles at the initial immersion time for the coated samples are corresponding to the zinc coating than the stainless steel substrate. Detecting such low impedance response at longer immersion times can indicate the existence and confirm the durability of the applied coating on each sample.

Nevertheless, after 72 h of immersion time (Figure 21b), for the coated ground and coated sandblasted surfaces, the electrolyte solution gradually penetrated to the coating and zinc has started to preferentially dissolve to the solution, leaving some areas uncoated and exposed to the solution, causing an increase in the impedance values at the lower frequency range in the Bode diagram (values in the range of 10^4 Ωcm^2). Also, the maximum phase angle shifted to lower frequencies. Therefore, after 72 h of immersion time in 3.5 wt.% NaCl electrolyte, the coated sandblasted and ground surfaces revealed a significant degradation of their hydrophobic coating, associated with penetration of the electrolyte into the coating and creating a path to the underlying surface along with dissolution of zinc layer to the electrolyte. However, the coated as-received sample shows almost the same impedance value after 72 h of immersion, confirming the stronger adhesion of the coating on its surface due to its optimum surface roughness (4.62±0.15 μm).

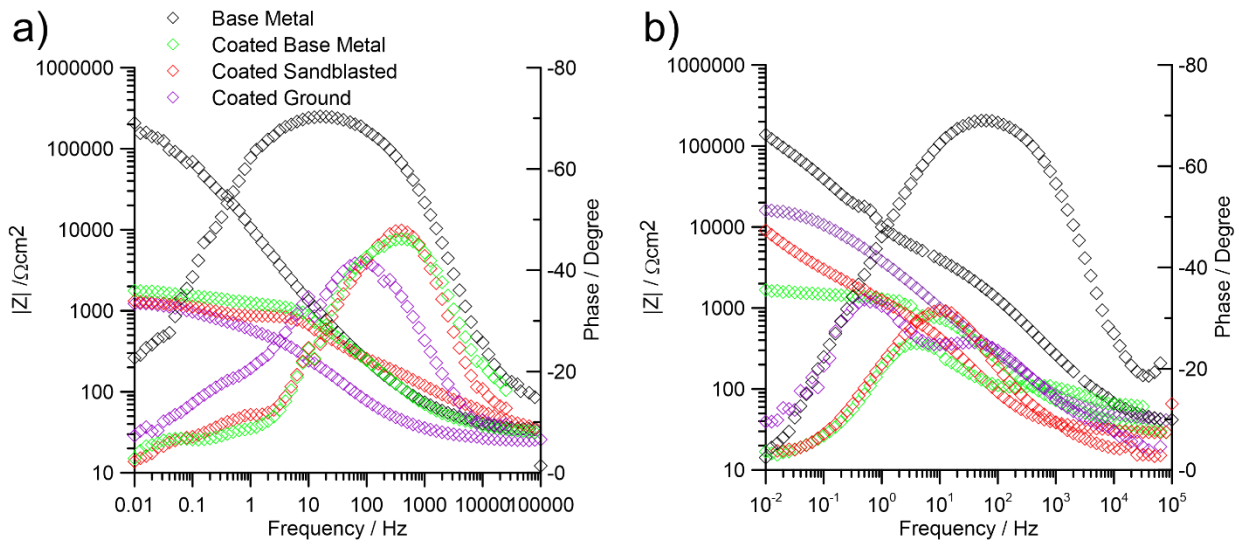

Figure 21. EIS spectra of the as-received base metal and all coated surfaces in aerated 3.5 wt.% NaCl solution after a) 1 h and b) 72 h of immersion time.

To study the electrochemical behavior of all samples and also the adhesion durability of the coating on the surface exposed to a continuous stream of salt spray, cyclic polarization tests were conducted on the samples after salt spray testing at various exposure time, and the results are shown in Figure 22. The electrochemical parameters extracted from the polarization graphs are presented in Table 2.

At the initial exposure time (up to 24 h), the cyclic polarization graphs showed a clear shift of corrosion potential towards more negative values for coated samples, corresponding to the higher tendency of the Zn coating layer for corrosion reactions as compared to the stainless steel. Moreover, the re-passivation potential (Erep.) was found to be lower than the corrosion potential (Ecorr.) for the coated samples, confirming the existence of a Zn coating with weaker repassivation properties relative to the base metal, which makes it susceptible to stable pit growth.

By increasing the salt spray exposure time to 72 h or 120 h, the coating is gradually removed from the substrate, and therefore, the substrate is exposed to the corrosive environment. After 72

h of salt spraying, the corrosion and pitting potential values for both coated and non-coated samples were measured to be approximately the same, confirming the chemical composition similarities of both exposed surfaces, which implies the hydrophobic coating has been entirely removed from the substrate after almost 72 h. Although the coated as-received sample revealed the coating stability even after 72 h of immersion in aerated 3.5 wt.% NaCl electrolyte at room temperature, the salt spray testing of the coated as-received samples revealed a complete detachment and dissolution of the coating after 72 h of testing. This is ascribed to the harsher salt spraying testing environment primarily due to the constant stress imposed on the sample's surface during the test.

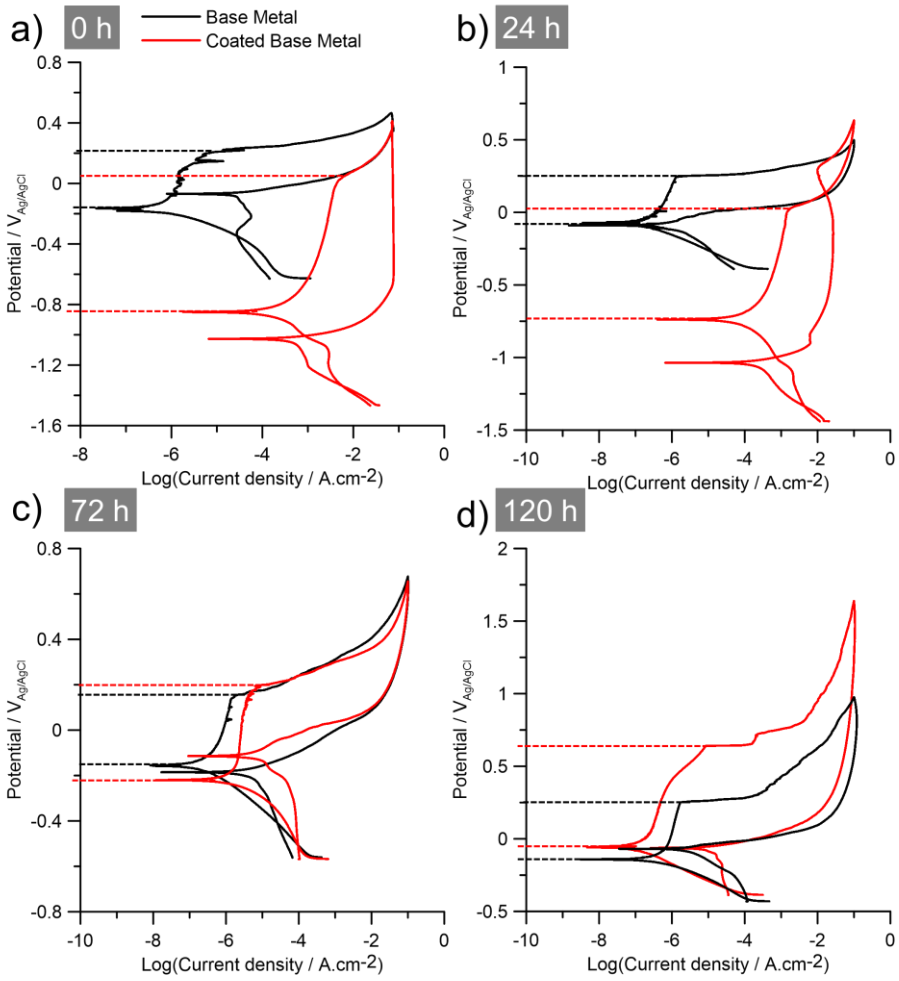

Figure 22. Cyclic polarization plots of the as-received base metal and coated base metal after a) 0 h, b) 24 h, c) 72 h, and d) 120 h of testing in the salt spray chamber.

Table 4. Polarization parameters deducted from the cyclic polarization plots shown in Figure 22.

Sample	Potential ($V_{Ag/AgCl}$)	0 h	24 h	72 h	120 h
As-received	E_{pit}	0.232	0.251	0.151	0.252
	E_{Corr}	- 0.166	-0.073	-0.162	-0.144
Coated as-received	E_{pit}	0.064	0.034	0.201	0.625
	$E_{Corr.}$	-0.848	-0.741	-0.221	-0.053

In addition to the CPP testing, EIS testing in aerated 3.5 wt.% NaCl electrolyte was also conducted after 24 h, 72 h, and 120 h of salt spray testing. The obtained EIS spectra for the as-received and coated as-received surfaces are presented in Figure 23. Analogous to the CPP results, after 24 h of exposure time, an extremely low impedance response was detected from the coated sample while the uncoated base metal did not reveal a noticeable change as compared to the sample's EIS response prior to the salt spraying testing (Figure 21a). Therefore, consistent with the CPP results after 24 h of salt spraying testing, the existence of the protective hydrophobic coating was confirmed, indicated by the detected low impedance and phase angle response of the Zn coating on the EIS spectra. After longer exposure times, *i.e.* 72 h and 120 h, the Bode plots (Figures 23b and 23c, respectively) revealed a significant increase of both impedance and the phase angles of the coated as-received sample to values very close to the uncoated base metal, corresponding to the entire detachment of the applied hydrophobic coatings from the samples surfaces. This is also in agreement with the CPP plots of the samples after 72 h and 120 h of exposure time (shown in Figures. 22c and 22d, respectively).

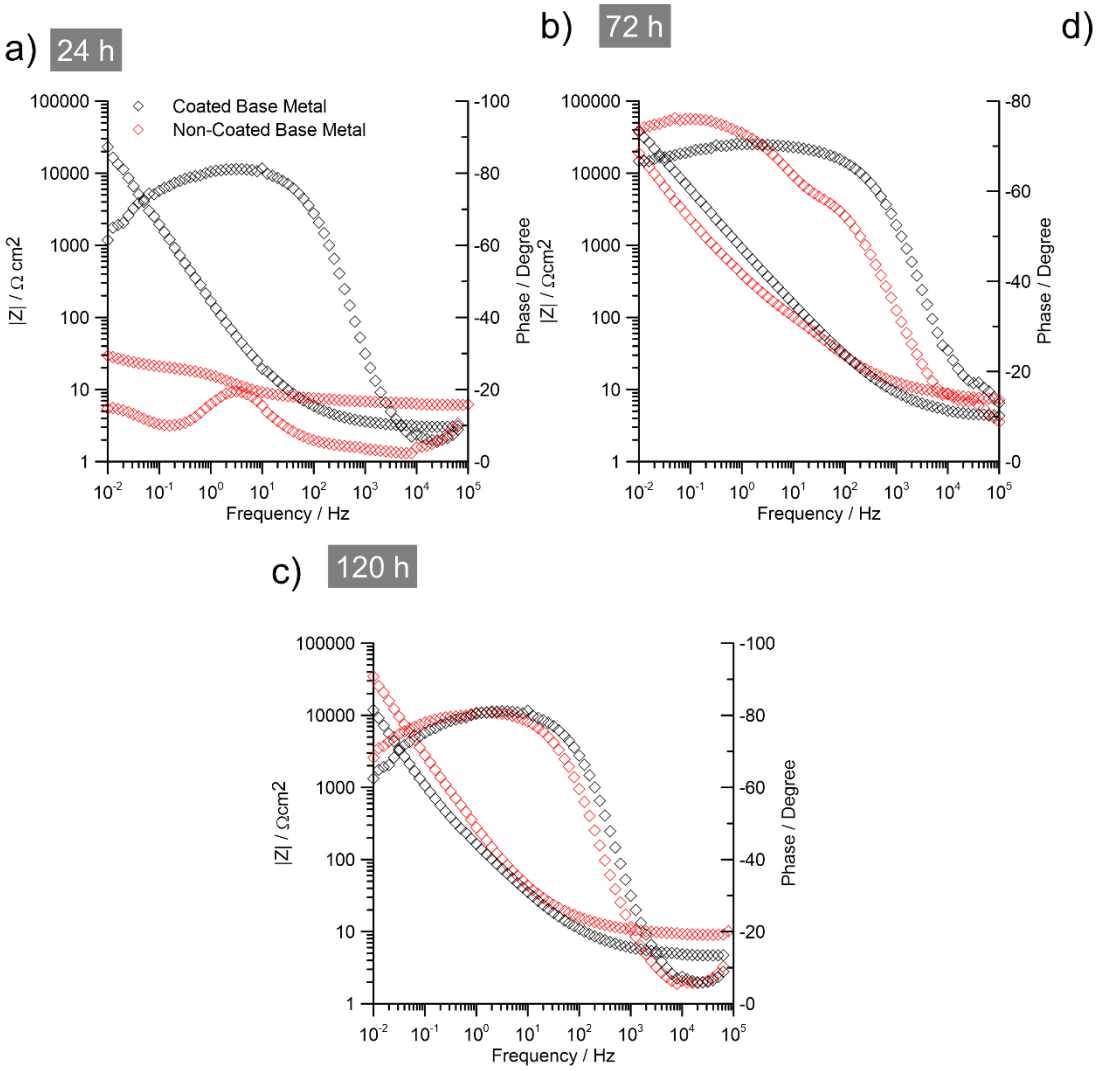

Figure 23. spectra of the as-received base metal and the coated as-received base metal surfaces in aerated 3.5 wt.% NaCl solution after a) 24 h, b) 72 h, and c) 120 h of salt spray testing..

Figure 24 shows the corrosion morphology of the coated and non-coated as-received surfaces after salt-spray exposure test and removing the corrosion products. As clearly depicted from Figure 24a, corrosion pits were not detected on the corroded surface of the as-received sample, while the non-coated as-received sample indicated pits formation on the entire corroded surface after salt spray test (Figure 24b). The coated as-received surface also revealed a minor corrosion attack after

72 h and 120 h of the exposure time (Figure 24c and 24e), with similar morphology to the 24 h sample. However, the non-coated surfaces show the more corrosion pits after exposing to the salt spray chamber (Figure 24d and 24f). The corrosion morphology of all fabricated surfaces was found to be consistent with the cyclic polarization and EIS behavior of the samples, revealing a more severe pitting corrosion attack on the non-coated as-received surface, as opposed to the coated as-received surface with a lower tendency to pitting in a simulated marine environment.

Therefore, the adhesion durability and corrosion behavior of the electrodeposited surfaces herein can be rationalized by considering the combined effects of the surface roughness, and super-hydrophobicity of the surfaces. Among all these factors, surface roughness has a prominent influence on the adhesion of the coating on the samples' surfaces. As a general trend, it is known that an optimum surface roughness finish gives rise to better coating durability and greater corrosion performance, as too smooth or roughened surfaces would lead to a drop in the durability of the coating, and consequently decrease the corrosion performance of the surfaces.

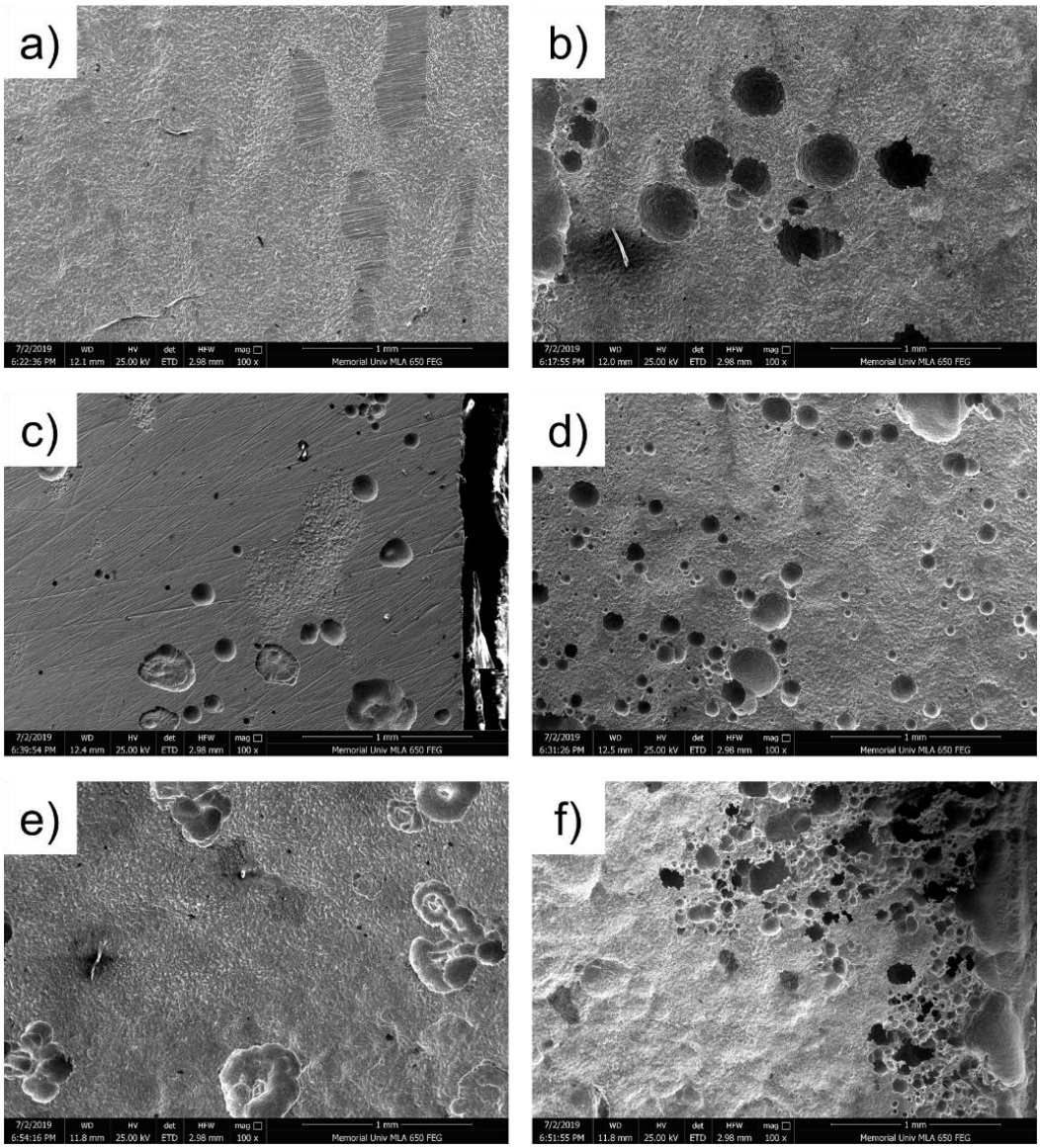

Figure 24. SEM micrographs of the coated as-received 17-4 PH stainless steel surface after a) 24 h, c) 72 h, e) 120 h, and non-coated as-received after b) 24 h, d) 72 h, f) 120 h of salt spray exposure.

CHAPTER 6

6. Conclusions, Future Works, and Recommendations

6.1. Conclusions

In the first project, hydrophobic and super-hydrophobic 17-4 PH stainless steel surfaces were successfully fabricated using different surface finishing procedures, including sandblasting, grinding, and polishing, followed by applying a super-hydrophobic coating to the surfaces. The samples showed hydrophobic or super-hydrophobic properties depending on the obtained surface roughness prior to applying the coating. The resulted hydrophobic and super-hydrophobic properties of the fabricated samples were associated with the combined effects of the surface roughness and low surface energy correlated to the super-hydrophobic coating. The coating could only increase the static contact angle of water droplets on the as-received base metal up to 140°; while by polishing and grinding of the surface, the contact angle was increased up to 146° and 152°, respectively, just around the necessary contact angle for super-hydrophobicity (150°).

To evaluate the corrosion performance and electrochemical stability of the fabricated surfaces, both cyclic polarization testing and electrochemical impedance spectroscopy (EIS) in aerated 3.5 wt.% NaCl solution were conducted. According to the corrosion testing results, the hydrophobic nature of the coated base metal and coated sandblasted surfaces was not found effective in contributing to the corrosion protection capability of the stainless steel substrate. The lowest corrosion potential with the highest corrosion current density leading to the highest corrosion rate was measured on the coated base metal and coated sandblasted hydrophobic samples. On the other hand, the super-hydrophobic nature of the coated ground and coated polished 17-4 PH stainless steel surface was found competent in preventing the aggressive chloride ions from approaching

the substrate leading to the improved corrosion properties of the material. This can be attributed to the size of the fabricated sub-micron features on the surface, meaning the surface features created by grinding or polishing surface treatment are able to retain the entrapped air inside the roughened surface structure in fully immersed condition in the corrosive electrolyte. Overall, the coated ground and coated polished 17-4 PH stainless steel samples revealed better corrosion resistance than other fabricated surfaces in a simulated seawater medium.

In the second project super-hydrophobic 17-4 PH stainless steel surfaces were successfully fabricated by combining three steps of surface modifications, i.e. surface grinding or sandblasting versus the as-received surfaces, electrodeposition of zinc coating, followed by coating the surface with stearic acid. The impact of the substrate's initial surface roughness on the applied coating's quality, uniformity, and durability in simulated harsh marine environment was also investigated by comparing the ground, sandblasted, and as-received surfaces. All fabricated samples revealed super-hydrophobic properties regardless of the obtained surface roughness prior to applying the coatings.

To evaluate the coating quality and durability on the fabricated surfaces, cyclic polarization testing and electrochemical impedance spectroscopy (EIS) in aerated 3.5 wt.% NaCl solution, and salt spray testing were conducted. According to the results, the initial surface roughness prior to the zinc electrodeposition step was found to be a critical factor affecting the quality and uniformity of the applied coating and its adhesion durability in the studied harsh environments. The best coating durability with a uniform coverage of the 17-4 PH stainless steel substrate was obtained on the as-received sample with the initial surface roughness of 4.62±0.15 µm.

Moreover, the coated 17-4 PH stainless steel surfaces were found competent in preventing the aggressive chloride ions from approaching the substrate leading to the improved corrosion

properties of the material. Overall, the coated as-received 17-4 PH stainless steel sample revealed better coating adhesion and corrosion resistance than other fabricated surfaces in a simulated seawater medium.

6.2. Future works

Several suggestions related to this thesis work are shown below for further investigation: Besides random large scale surface roughness using sandblasting and grinding, systematic nanoscales surface roughness can be fabricated via micro-EDM to investigate the scale impacts on wettability and coating durability as compared with large scales surface roughness.

It has been already showed that the zinc electrodeposits are effective at self-cleaning water behavior and its impact on the corrosion resistance of the stainless steel. Therefore, anti-acing properties of the zinc-electrodeposition can also be investigated to have a comprehensive knowledge of the applicability of this coating on the marine environments.

It would be more interesting if the impact of surface roughness and Zn electrodeposition are investigated on the non-corrosion resistance materials, such as carbon steels. Therefore, changing the substrate can be a potential topic for further studies.

6.3. Recommendations

Considering the results from Chapters 4 and 5, the surface roughness was found as the primary factor driving the corrosion performance of the 17-4PH stainless steel as well as the coating adhesion. When a super hydrophobic polymeric-based coating, such as FluoroThane WT, is applied on the 17-4 PH stainless steel surfaces, the smoother surface of the stainless steel, *i.e.* ground and polished ones with R_a value of 0.02±0.004 μm and 0.03±0.002 μm, respectively, show better corrosion performance.

Differently, the Zn electrodeposition of the 17-4 PH stainless steel can be more effective at the substrate's optimum surface roughness of 4.62 ± 0.15 μm (corresponding to the as-received substrate with no surface preparation), leading to a better coating adhesion and durability, resulting in the improved corrosion performance of the 17-4PH stainless steel surface.

References

[1] A. M. A. Mohamed, A. M. Abdullah, and N. A. Younan, "Corrosion Behavior of Superhydrophobic Surfaces: A Review," *Arab. J. Chem.*, vol. 8, no. 6, pp. 749–765, Nov. 2015.

[2] J. Simpson, S. Hunter, and T. Aytug, "Superhydrophobic Materials and Coatings: A Review," *Rep. Prog. Phys.*, vol. 78, p. 86501, 2015.

[3] C. Cui, X. Duan, B. Collier, and K. M. Poduska, "Fabrication and Wettability Analysis of Hydrophobic Stainless Steel Surfaces With Microscale Structures From Nanosecond Laser Machining," *J. Micro Nano-Manufacturing*, vol. 6, no. 3, pp. 31006–31008, Jun. 2018.

[4] M. Rafieazad, J. A. Jaffer, C. Cui, X. Duan, and A. Nasiri, "Nanosecond Laser Fabrication of Hydrophobic Stainless Steel Surfaces: The Impact on Microstructure and Corrosion Resistance," *Materials (Basel).*, vol. 11, no. 9, p. 1577, 2018.

[5] M. Amiriafshar, X. Duan, and A. Nasiri, "Fabrication and Corrosion Performance of a Superhydrophobic Stainless Steel Surface," in *17 th International Conference on Nanochannels, Microchannels, and Minichannels*, 2019, p. 4209.

[6] T. Limongi *et al.*, "Photolithography and Micromolding Techniques for the Realization of 3D Polycaprolactone Scaffolds for Tissue Engineering Applications," *Microelectron. Eng.*, vol. 141, pp. 135–139, Jun. 2015.

[7] B. Gao and K. Poduska, "Electrodeposited Zn for Water-Repellent Coatings," *J. Electrochem. Soc.*, vol. 165, pp. D472–D476, 2018.

[8] A. Rodriguez *et al.*, "Laser Interference Lithography for Nanoscale Structuring of Materials: From Laboratory to Industry," *Microelectron. Eng.*, vol. 86, no. 4–6, pp. 937–

940, Apr. 2009.

[9] Y. Liu, X. Yin, J. Zhang, Y. Wang, Z. Han, and L. Ren, “Biomimetic Hydrophobic Surface Fabricated by Chemical Etching Method from Hierarchically Structured Magnesium Alloy Substrate,” *Appl. Surf. Sci.*, vol. 280, pp. 845–849, Sep. 2013.

[10] D. J. Abson and R. J. Pargeter, “Factors Influencing As-deposited Strength, Microstructure, and Toughness of Manual Metal Arc Welds Suitable for C-Mn Steel Fabrications,” *Int. Mater. Rev.*, vol. 31, no. 1, pp. 141–196, Jan. 1986.

[11] S. Yuan, S. O. Pehkonen, B. Liang, Y. P. Ting, K. G. Neoh, and E. T. Kang, “Superhydrophobic Fluoropolymer-modified Copper Surface via Surface Graft Polymerisation for Corrosion Protection,” *Corros. Sci.*, vol. 53, no. 9, pp. 2738–2747, Sep. 2011.

[12] E. Geler and D. S. Azambuja, “Corrosion Inhibition of Copper in Chloride Solutions by Pyrazole,” *Corros. Sci.*, vol. 42, no. 4, pp. 631–643, 2000.

[13] R. L. Brown, “A review of: ‘Steels: Heat Treatment and Processing Principles,’” *Mater. Manuf. Process.*, vol. 6, no. 3, pp. 569–570, 1991.

[14] F. C. Campbell, *Elements of Metallurgy and Engineering Alloys*. ASM International, 2008.

[15] J. Kazior, A. Szewczyk-Nykiel, T. Pieczonka, M. Hebda, and M. Nykiel, “Properties of Precipitation Hardening 17-4 PH Stainless Steel Manufactured by Powder Metallurgy Technology,” *Adv. Mater. Res.*, vol. 811, pp. 87–92, 2013.

[16] W. D. Callister and D. G. Rethwisch, “Materials Science and Engineering : An Introduction,” 2019.

[17] D. A. Jones, *Principles and Prevention of Corrosion*. Prentice Hall, 1996.

[18] S. Papavinasam, “Electrochemical Polarization Techniques for Corrosion Monitoring,” in *Techniques for Corrosion Monitoring*, L. Yang, Ed. Woodhead Publishing, 2008, pp. 49–85.

[19] P. L. Bonora, F. Deflorian, L. Fedrizzi, and S. Rossi, “Electrochemical Evalution of Coatings for Marine Corrosion Control,” in *Developments in Marine Corrosion*, S. A. Campbell, N. Campbell, and F. C. Walsh, Eds. Woodhead Publishing, 1998, pp. 163–180.

[20] K. A. Chandler, “Paint Coatings,” in *Marine and Offshore Corrosion*, K. A. Chandler, Ed. Butterworth-Heinemann, 1985, pp. 204–232.

[21] Z. Ahmad, A. U. Khan, R. Farooq, N. R. Mastoi, and T. Saif, “Hydrophobicity A Green Technique for Enhancing Corrosion Resistance of Alloys,” in *New Trends in Alloy Development, Characterization and Application*, InTech, 2015.

[22] S. Khorsand, K. Raeissi, and F. Ashrafizadeh, “Corrosion Resistance and Long-term Durability of Super-hydrophobic Nickel Film Prepared by Electrodeposition Process,” *Appl. Surf. Sci.*, vol. 305, pp. 498–505, Jun. 2014.

[23] G. Sander *et al.*, “Corrosion of Additively Manufactured Alloys: A Review,” *Corrosion*, vol. 74, no. 12, pp. 1318–1350, 2018.

[24] T. Young, “An Essay on the Cohesion of Fluids,” *Philos. Trans. R. Soc. London*, vol. 95, pp. 65–87, 1805.

[25] T. Nishino, M. Meguro, K. Nakamae, M. Matsushita, and Y. Ueda, “The Lowest Surface Free Energy Based on -CF3 Alignment,” *Langmuir*, vol. 15, no. 13, pp. 4321–4323, 1999.

[26] H. Margenau, “Surface Energy of Liquids,” *Phys. Rev.*, vol. 38, no. 2, pp. 365–371, Jul. 1931.

[27] A. J. Meuler, G. H. McKinley, and R. E. Cohen, “Exploiting Topographical Texture To

Impart Icephobicity," *ACS Nano*, vol. 4, no. 12, pp. 7048–7052, 2010.

[28] M. J. Kreder, J. Alvarenga, P. Kim, and J. Aizenberg, "Design of Anti-icing Surfaces: Smooth, Textured or Slippery?," *Nat. Rev. Mater.*, vol. 1, p. 15003, Jan. 2016.

[29] C. Neinhuis and W. Barthlott, "Characterization and Distribution of Water-repellent, Self-cleaning Plant Surfaces," *Ann. Bot.*, vol. 79, pp. 667–677, 1997.

[30] F. Müller, C. Kunz, and S. Gräf, "Bio-Inspired Functional Surfaces Based on Laser-Induced Periodic Surface Structures," *Materials (Basel).*, vol. 9, no. 6, p. 476, Jun. 2016.

[31] P. Ke and W. Xinxin, "Super-cooled Large Droplets consideration in the droplet impingement simulation for aircraft icing," *Procedia Eng.*, vol. 17, pp. 151–159, 2011.

[32] R. Karmouch, S. Coudé, G. Abel, and G. G. Ross, "Icephobic PTFE Coatings for Wind Turbines Operating in Cold Climate Conditions," in *2009 IEEE Electrical Power & Energy Conference (EPEC)*, 2009, pp. 1–6.

[33] W. Barthlott and C. Neinhuis, "Purity of the Sacred Lotus, or Escape from Contamination in Biological Surfaces," *Planta*, vol. 202, no. 1, pp. 1–8, Apr. 1997.

[34] S. Nishimoto and B. Bhushan, "Bioinspired Self-cleaning Surfaces with Superhydrophobicity, Superoleophobicity, and Superhydrophilicity," *RSC Adv.*, vol. 3, no. 3, pp. 671–690, 2013.

[35] P. S. Virk, "Drag Reduction Fundamentals," *AIChE J.*, vol. 21, no. 4, pp. 625–656, 1975.

[36] N. R. Geraldi *et al.*, "Drag Reduction Properties of Superhydrophobic Mesh Pipes," *Surf. Topogr. Metrol. Prop.*, vol. 5, no. 3, p. 34001, Jul. 2017.

[37] H. Tian, J. Zhang, E. Wang, Z. Yao, and N. Jiang, "Experimental investigation on drag reduction in turbulent boundary layer over superhydrophobic surface by TRPIV," *Theor. Appl. Mech. Lett.*, vol. 5, no. 1, pp. 45–49, 2015.

[38] R. Truesdell, A. Mammoli, P. Vorobieff, F. van Swol, and C. J. Brinker, “Drag Reduction on a Patterned Superhydrophobic Surface,” *Phys. Rev. Lett.*, vol. 97, no. 4, p. 44504, Jul. 2006.

[39] L. B. Boinovich, A. M. Emelyanenko, A. D. Modestov, A. G. Domantovsky, and K. A. Emelyanenko, “Synergistic Effect of Superhydrophobicity and Oxidized Layers on Corrosion Resistance of Aluminum Alloy Surface Textured by Nanosecond Laser Treatment.,” *ACS Appl. Mater. Interfaces*, vol. 7, no. 34, pp. 19500–19508, Sep. 2015.

[40] W. F. Ng, M. H. Wong, and F. T. Cheng, “Stearic Acid Coating on Magnesium for Enhancing Corrosion Resistance in Hanks’ Solution,” *Surf. Coatings Technol.*, vol. 204, no. 11, pp. 1823–1830, 2010.

[41] S. S. Latthe *et al.*, “A Mechanically Bendable Superhydrophobic Steel Surface with Self-cleaning and Corrosion-Resistant Properties,” *J. Mater. Chem. A*, vol. 3, no. 27, pp. 14263–14271, 2015.

[42] B. Park and W. Hwang, “A facile Fabrication Method for Corrosion-resistant Micro/Nanostructures on Stainless Steel Surfaces with Tunable Wettability,” *Scr. Mater.*, vol. 113, pp. 118–121, Mar. 2016.

[43] U. Trdan, M. Hočevar, and P. Gregorčič, “Transition from Superhydrophilic to Superhydrophobic State of Laser Textured Stainless Steel Surface and its Effect on Corrosion Resistance,” *Corros. Sci.*, vol. 123, pp. 21–26, Jul. 2017.

[44] H. Ogihara, J. Xie, and T. Saji, “Factors Determining Wettability of Superhydrophobic Paper Prepared by Spraying Nanoparticle Suspensions,” *Colloids Surfaces A Physicochem. Eng. Asp.*, vol. 434, no. Supplement C, pp. 35–41, 2013.

[45] F. J. Montes Ruiz-Cabello, A. Amirfazli, M. Cabrerizo-Vílchez, and M. A. Rodríguez-

Valverde, “Fabrication of Water-repellent Surfaces on Galvanized Steel,” *RSC Adv.*, vol. 6, no. 76, pp. 71970–71976, 2016.

[46] S. Yu, X. Wang, W. Wang, Q. Yao, J. Xu, and W. Xiong, “A New Method for Preparing Bionic Multi Scale Superhydrophobic Functional Surface on X70 Pipeline Steel,” *Appl. Surf. Sci.*, vol. 271, pp. 149–155, 2013.

[47] D. J. Varacalle, D. P. Guillen, D. M. Deason, W. Rhodaberger, and E. Sampson, “Effect of Grit-blasting on Substrate Roughness and Coating Adhesion,” *J. Therm. Spray Technol.*, vol. 15, no. 3, pp. 348–355, Sep. 2006.

[48] T. Xiang *et al.*, “A facile Method for Fabrication of Superhydrophobic Surface with Controllable Water Adhesion and its Applications,” *J. Alloys Compd.*, vol. 704, pp. 170–179, 2017.

[49] F. Berger, J. Delhalle, and Z. Mekhalif, “Undec-10-ene-1-thiol Multifunctional Molecular Layer as a Junction between Metallic Zinc and Polymer Coatings on Steel,” *Electrochim. Acta*, vol. 54, no. 26, pp. 6464–6471, 2009.

[50] Y. S. Wong, M. Rahman, H. S. Lim, H. Han, and N. Ravi, “Investigation of Micro-EDM Material Removal Characteristics Using Single RC-pulse Discharges,” *J. Mater. Process. Technol.*, vol. 140, no. 1, pp. 303–307, 2003.

[51] W. G. Bae *et al.*, “One-Step Process for Superhydrophobic Metallic Surfaces by Wire Electrical Discharge Machining,” *ACS Appl. Mater. Interfaces*, vol. 4, no. 7, pp. 3685–3691, 2012.

[52] R. S. C. Paredes, S. C. Amico, and A. S. C. M. D’Oliveira, “The Effect of Roughness and Pre-heating of the Substrate on the Morphology of Aluminium Coatings Deposited by Thermal Spraying,” *Surf. Coat. Technol.*, vol. 200, no. 9, pp. 3049–3055, 2006.

[53] L. Slatineanu, Ş. Potârniche, M. Coteata, I. Besliu, L. Gherman, and F. Negoescu, "Surface Roughness at Aluminum Parts Sandblasting," *Proceeding Manuf. Syst.*, vol. 6, no. 2, pp. 69–74, 2011.

[54] Y. Fan, Y. He, P. Luo, X. Chen, and B. Liu, "A Facile Electrodeposition Process to Fabricate Corrosion-Resistant Superhydrophobic Surface on Carbon Steel," *Appl. Surf. Sci.*, vol. 368, pp. 435–442, 2016.

[55] G. Zheng, B. N. Popov, and R. E. White, "Use of Underpotential Deposition of Zinc to Mitigate Hydrogen Absorption into Monel K500," *J. Electrochem. Soc.*, vol. 141, no. 5, pp. 1220–1224, 1994.

[56] A. Y. Hosny, M. E. El-Rafei, T. A. Ramadan, B. A. El-Gafari, and S. M. Morsy, "Corrosion Resistance of Zinc Coatings Produced from a Sulfate Bath," *Met. Finish.*, vol. 93, no. 11, pp. 55–59, 1995.

[57] H. H. Lee and D. Hiam, "Corrosion Resistance of Galvannealed Steel," *Corrosion*, vol. 45, no. 10, pp. 852–856, 1989.

[58] N. P. Klochko *et al.*, "On Controlling the Hydrophobicity of Nanostructured Zinc-Oxide Layers Grown by Pulsed Electrodeposition," *Semiconductors*, vol. 50, no. 3, pp. 352–363, Mar. 2016.

[59] X. Zhang, J. Liang, B. Liu, and Z. Peng, "Preparation of Superhydrophobic Zinc Coating for Corrosion Protection," *Colloids Surfaces A Physicochem. Eng. Asp.*, vol. 454, pp. 113–118, 2014.

[60] T. Ning, W. Xu, and S. Lu, "Fabrication of Superhydrophobic Surfaces on Zinc Substrates and their Application as Effective Corrosion Barriers," *Appl. Surf. Sci.*, vol. 258, no. 4, pp. 1359–1365, Dec. 2011.

[61] Tegramin-30, “Struers.”

[62] S. Edge, “Vaniman 80410.” [Online]. Available: https://www.vaniman.com/product/sandstorm-edge-80410/.

[63] Cytonix, “FluoroThane WT,” *Manufacturer of hydrophobic & oleophobic coating, additive & inks*. [Online]. Available: https://www.cytonix.com/. [Accessed: 21-Aug-2018].

[64] J. Vazquez-Arenas, F. Sosa-Rodriguez, I. Lazaro, and R. Cruz, “Thermodynamic and Electrochemistry Analysis of the Zinc Electrodeposition in NH4Cl–NH3 Electrolytes on Ti, Glassy Carbon and 316L Stainless Steel,” *Electrochim. Acta*, vol. 79, pp. 109–116, 2012.

[65] D. Instrument, “OCA – Optical Contact Angle Measuring and Contour Analysis.”

[66] A. S. Materials, *ASTM G5-14: Standard Reference Test Method for Making Potentiodynamic Anodic Polarization Measurements*. ASTM, 2014.

[67] “Standard Practice for Operating Salt Spray (Fog) Apparatus.” 18AD.

[68] T. K. Rout and N. Bandyopadhyay, “Effect of Molybdate Coating for White Rusting Resistance on Galvanized Steel,” *Anti-Corrosion Methods Mater.*, vol. 54, no. 1, pp. 16–20, Jan. 2007.

[69] E. P. (Ernest P. DeGarmo, J. T. Black, and R. A. Kohser, *Materials and Processes in Manufacturing*, 9th ed.,In. New York ; Chichester : Wiley, 2003.

[70] A. B. D. Cassie and S. Baxter, “Wettability of Porous Surfaces,” *Trans. Faraday Soc.*, vol. 40, pp. 546–551, 1944.

[71] N. Wang and D. Xiong, “Superhydrophobic Membranes on Metal Substrate and their Corrosion Protection in Different Corrosive Media,” *Appl. Surf. Sci.*, vol. 305, pp. 603–

608, Jun. 2014.

[72] L. Chen, “The Corrosion Behavior of 17-4 Stainless Steel in a Stainless Steel-Carbon Steel Galvanic Couple,” *Int. J. Electrochem. Sci.*, vol. 12, pp. 9445–9455, 2017.

[73] A. V. C. Sobral, W. Ristow, O. V. Correa, C. V Franco, and I. Costa, “Corrosion Behaviour of Injection Moulded 316L and 17-4PH Stainless Steels in a Sodium Chloride Solution,” in *Advanced Powder Technology II*, 2001, vol. 189, pp. 667–672.

[74] T. Hong and M. Nagumo, “Effect of surface roughness on early stages of pitting corrosion of Type 301 stainless steel,” *Corros. Sci.*, vol. 39, no. 9, pp. 1665–1672, Sep. 1997.

[75] S. Yin and D. Y. Li, “Effects of Prior Cold Work on Corrosion and Corrosive Wear of Copper in HNO3 and NaCl Solutions,” *Mater. Sci. Eng. A*, vol. 394, no. 1, pp. 266–276, 2005.

[76] U. K. Mudali, P. Shankar, S. Ningshen, R. K. Dayal, H. S. Khatak, and B. Raj, “On the Pitting Corrosion Resistance of Nitrogen Alloyed cold Worked Austenitic Stainless Steels,” *Corros. Sci.*, vol. 44, no. 10, pp. 2183–2198, 2002.

[77] X. Liu, J. Xiong, Y. Lv, and Y. Zuo, “Study on Corrosion Electrochemical Behavior of Several Different Coating Systems by EIS,” *Prog. Org. Coatings*, vol. 64, no. 4, pp. 497–503, 2009.

[78] Y. Li, “Electrochemical Study of Corrosion Behavior of Stellite 6 Alloy and 17-4PH Stainless Steel in Amine Solutions,” Carleton University, 2017.

[79] A. V. C. Sobral, C. V Franco, O. V. Correa, and I. Costa, “Corrosion Resistance of Powder Injection Moulded AISI 316L and 17-4PH Stainless Steels in Acid Rain Environments,” in *Advanced Powder Technology III*, 2003, vol. 416, pp. 64–69.

[80] G. Reinhard, P. Simon, and U. Rammelt, “Application of Corrosion Inhibitors in Water-

borne Coatings," *Prog. Org. Coatings*, vol. 20, no. 3, pp. 383–392, 1992.

[81] E. S. Gadelmawla, M. M. Koura, T. M. A. Maksoud, I. M. Elewa, and H. H. Soliman, "Roughness Parameters," *J. Mater. Process. Technol.*, vol. 123, no. 1, pp. 133–145, 2002.